

Protein Friction and Filament Bending Facilitate Contraction of Disordered Actomyosin Networks

Alexander K. Y. Tam^{*1}, Alex Mogilner², and Dietmar B. Oelz¹

¹School of Mathematics and Physics, The University of Queensland, St Lucia, Queensland 4072, Australia

²Courant Institute of Mathematical Sciences, New York University, New York, NY 10012, USA

June 18, 2021

Abstract

We use mathematical modelling and computation to investigate how protein friction facilitates contraction of disordered actomyosin networks. We simulate two-dimensional networks using an agent-based model, consisting of a system of force-balance equations for myosin motor proteins and semi-flexible actin filaments. A major advantage of our approach is that it enables direct calculation of the network stress tensor, which provides a quantitative measure of contractility. Exploiting this, we use repeated simulations of disordered networks to confirm that both protein friction and actin filament bending are required for contraction. We then use simulations of elementary two-filament assemblies to show that filament bending flexibility can **facilitate** contraction on the microscopic scale. Finally, we show that actin filament turnover is necessary to sustain contraction and prevent **filament aggregation**. Simulations with and without turnover also exhibit contractile pulses. However, these pulses are aperiodic, suggesting that periodic pulsation can only **arise due to additional regulatory mechanisms or more complex mechanical behaviour**.

Keywords: Actin, myosin, energy functional, stress tensor, turnover

1 Introduction

The mechanics of actomyosin networks govern essential cellular processes, including muscle contraction [1], cell division [2], and cell motility [3]. Assemblies of actin and myosin exhibit diverse structural organisation. In muscles, actin filaments are aligned in parallel to form sarcomeres, in which myosin-II motor proteins generate force in accordance with the sliding filament theory [1]. Alternatively, actin filaments form a disordered two-dimensional meshwork in the cell cortex, located below the membrane of living cells. These filaments are cross-linked by myosin motors, which exert forces that give rise to cortical tension

^{*}Corresponding author: alex.tam@uq.edu.au

9 and flow [4]. This cortex deformation subsequently determines cellular morphology and
 10 locomotion. Understanding the mechanisms by which myosin motors generate local forces
 11 is challenging, and can be investigated using mathematical modelling and computation.

12 The sliding filament mechanism provides a starting point for investigating contraction
 13 in disordered networks. Myosin motors attached to pairs of parallel actin filaments can
 14 generate either contraction or expansion, depending on filament orientation. A motor
 15 protein bound to a pair of filaments with barbed ends facing outwards will generate local
 16 contraction, as shown in panel A of Figure 1. Conversely, the filaments generate expansion
 17 if pointed ends face outwards (Figure 1, panel B). However, this sliding filament mechanism
 18 alone cannot explain net contraction in disordered networks, in which filaments can cross
 19 at arbitrary angles and in either configuration with equal probability. In these networks,
 20 there must be additional symmetry-breaking mechanisms that favour contraction over
 21 expansion.

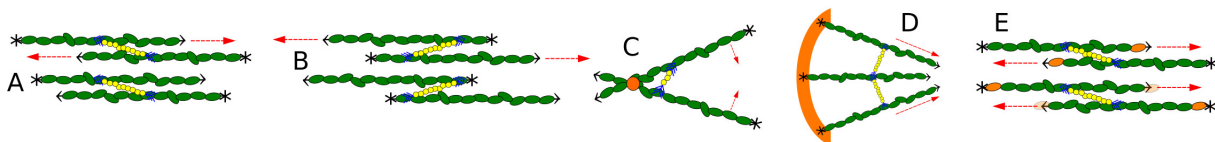


Figure 1: Schematic representations of (A): contraction via the sliding filament mechanism, (B): expansion via the sliding filament mechanism, (C): filament zippering, (D): filament anchoring, (E): actin treadmilling. Asterisks indicate filament barbed (plus) ends, arrow heads indicate pointed (minus) ends. Dashed arrows represent direction of filament movement.

22 Candidate mechanisms for generating contraction in disordered networks fall into the
 23 broad categories of structural and force asymmetries. Structural asymmetries break the
 24 random alignment of actin and myosin, enabling contractile configurations to emerge
 25 more often than expansive ones. Force asymmetries arise if filaments behave differently
 26 under tension and compression, enabling contraction more readily than expansion. In
 27 cells, mechanisms of contraction can be redundant and act as fail-safes in case network
 28 components are absent or lose function [5–7]. Many contractile mechanisms have been
 29 proposed and investigated for this reason.

30 Several hypotheses exist for generating structural asymmetries in two-dimensional
 31 networks. One example is a zippering mechanism, whereby a motor with non-zero length
 32 is displaced ahead of the intersection between two filaments (see Figure 1, panel C). Motor
 33 movement towards the plus ends then pulls the filaments inwards, generating contraction
 34 [8–10]. Theoretical work by Lenz [9] showed that zippering can generate net contraction
 35 in disordered networks, but is unlikely to occur in practice. Another possible structural
 36 asymmetry is based on the observation that some filaments grow with barbed ends anchored
 37 to the cell membrane [5, 6] (see Figure 1, panel D). Contraction can then occur via the

38 sliding filament mechanism, since the anchored filaments are in a contractile alignment.
39 However, a drawback of this hypothesis is that only a small fraction of filaments in the
40 cortex are anchored, such that non-anchored filaments are thought to play a major role in
41 contractility [6]. A third hypothesised structural asymmetry for generating contraction is
42 actin treadmilling, which involves simultaneous filament depolymerisation at minus ends
43 and polymerisation at plus ends [11]. This enables contractile structures to persist as
44 barbed ends are pulled inwards, generating a structural asymmetry (see Figure 1, panel E).
45 Oelz, Rubinstein, and Mogilner [12] showed that treadmilling gives rise to network-scale
46 contraction in one-dimensional ring-like geometry. Previous theoretical work has also
47 shown that myosin motors lingering at filament barbed ends instead of unbinding can
48 generate contraction [9, 13, 14]. However, although this behaviour has been observed in
49 experiments, it is not known whether it occurs in non-muscle cells [15].

50 In contrast to these structural asymmetries, many studies consider a mechanism
51 whereby filaments can sustain tension, but buckle under compression. The resulting
52 asymmetric force propagation favours contraction. This has been illustrated *in vitro* [16]
53 as well as theoretically [17] by suggesting that filaments nullify expansion by buckling
54 when they are longer than a threshold length. Filament bending is likely to be relevant
55 in cellular actomyosin, because the forces exerted by myosin motors are large enough to
56 bend filaments with lengths below 1 μm [16], which is the approximate filament length [18].
57 However, the forces required to initiate bending are approximately 1000 times smaller than
58 those required to rupture filaments [19]. Therefore, filament bending without severing
59 might also play a role in contraction.

60 Mathematical modelling has facilitated advancements in understanding actomyosin
61 contraction. One phenomenological approach is to treat the actomyosin network as an
62 active gel continuum [13, 20]. In these models, filament and motor positions are expressed
63 in terms of continuous density fields. Although these models can effectively predict pattern
64 formation in actomyosin networks [21], many recent models focus on developing accurate
65 microscopic descriptions of network components. Since we are interested in whether actin
66 filament bending can induce contraction on both the microscopic and network scales, we
67 focus on coarse-grained agent-based models. These models use simplified representations of
68 individual network components, and track how they evolve over time. Agent-based models
69 enable detailed description of the mechanics on a microscopic scale, and can subsequently
70 be used to derive accurate continuum models [22].

71 Many agent-based models for the cytoskeleton exist, including publicly-available soft-
72 ware Cytosim [23], AFINES [24], and MEDYAN [25]. These, and many other authors [7,
73 26–29], use modified Brownian dynamics to simulate actomyosin networks. Under this
74 approach, actin filaments move according to an overdamped Langevin-like equation for

75 the balance of forces between network components [7, 23–29]. Within this framework,
76 many authors have recognised the importance of filament bending forces to contractility
77 [7, 14, 24, 30–33]. A common approach is to focus on filament buckling [17, 24, 31, 34,
78 35] as a mechanism of contraction. This represents an extreme case of force asymmetry
79 generated by deformable filaments. Using a one-filament worm-like chain model, Lenz [9]
80 showed that motor-induced filament bending can facilitate contraction, and is relevant for
81 typical experimental parameters. However, further quantitative analysis of this bending
82 force asymmetry in filament networks is required.

83 Protein friction can be represented as effective viscous drag that acts point-wise at
84 the binding site of a motor or cross-linker, or at the point of contact between filaments
85 [36]. Using a one-dimensional model, Oelz, Rubinstein, and Mogilner [12] showed that a
86 combination of actin treadmilling and drag distributed along filament pairs that overlap
87 can contract a ring-like network of rigid filaments. In two-dimensions, protein friction
88 manifests as point-wise drag at filament intersections [37, 38]. McFadden et al. [38]
89 showed that point-wise drag and bending force asymmetry facilitate contraction. These
90 models with protein friction draw parallels between point-wise drag and cross-linkers
91 [37, 38]. However, this implies that cross-linkers are either short and abundant, or turn
92 over rapidly. The possibility of using point-wise drag to represent solid friction between
93 filaments remains largely unexplored, and additional work is required to determine how
94 this affects network contraction.

95 To address these research gaps, we develop a mathematical model for semi-flexible
96 actin filaments and myosin motors to investigate how protein friction affects contractility.
97 A promising simulation approach was developed by Dasanayake, Michalski, and Carlsson
98 [39], and Hiraiwa and Salbreux [10], where the network configuration is given by the
99 minimiser of a potential energy functional. However, these studies considered the evolution
100 of random networks to a steady state, and neglected longer-time evolution of the network.
101 In developing our model, we extend this approach to fully time-dependent simulations.

102 **2 Mathematical Model**

103 We develop an agent-based model to simulate two-dimensional disordered networks. The
104 network contains semi-flexible actin filaments, which we represent as finite-length curves
105 in two-dimensional space. We represent myosin motors as dumbbells that behave as linear
106 springs with equilibrium length zero, such that they attach to filament pairs at intersections.
107 We assume that myosin motors detach immediately if they reach a filament plus end,
108 and otherwise model force-dependent random detachment according to Bell’s law [40].
109 **Movement** of unattached motors **is not modelled explicitly**. Instead, we assume that a new

110 motor immediately attaches at a random filament intersection when an unbinding event
 111 occurs. **Although this is not representative of real networks, it enforces that the density of**
 112 **active motors remains constant. This ensures variation in the number of motors cannot**
 113 **influence the results.** We then **simulate network evolution by solving** for the positions of
 114 filament nodes and myosin motors on a square domain with periodic boundary conditions.

115 Components in cytoskeletal networks undergo continuous turnover [30, 41–43]. This
 116 refers to the exchange of filaments, motors, and cross-linkers between the network and
 117 cytoplasm [10]. Turnover can occur when filament sever [16] or undergo treadmilling [12,
 118 44, 45], which depend on motor [16] and cross-linker activity [34]. We explicitly model
 119 actin turnover by removing filaments (and any attached motors) at random with a constant
 120 rate [10, 38]. When a filament is removed, we immediately replace it with a new one at a
 121 random position, to maintain constant filament density. This represents a simple model
 122 for actin turnover, just as our treatment of myosin unbinding represents a simple model
 123 for motor turnover.

124 Protein friction is another mechanical feature that might influence network contractility
 125 [36, 46]. It can arise from binding and unbinding interactions between filaments and
 126 motors [46], filaments and cross-linkers [47], or from solid friction between filament pairs
 127 in contact [48]. Contact frictional forces are larger than hydrodynamic friction between
 128 filaments and the cytoplasm [47, 48], and have comparable magnitude to forces exerted
 129 by myosin motors [48]. In our model we apply viscous drag at intersections between
 130 actin filaments to model protein friction originating from either cross-linking or filament
 131 contact [37, 38]. We assume that presence of myosin motor prevents protein friction via
 132 cross-linking or filament contact, and do not apply point-wise drag between filament pairs
 133 connected to the same motor. Our model then enables investigation of whether protein
 134 friction, in conjunction with actin filament bending, **gives rise to** contraction.

135 We write the core model as a system of force-balance equations, which contains all
 136 mechanical features included in the model. In abstract terms, the system of equations is

$$\begin{aligned}
 \mathbf{0} = & \mathbf{F}_{a,\text{drag}} - \delta E_{a,\text{bend}} - \delta E_{a,\text{spring}} + \mathbf{F}_{a,\text{pf}} \\
 & - \delta E_{m,\text{spring}} + \mathbf{F}_{m,a}.
 \end{aligned}
 \tag{2.1}$$

138 Actin filaments contribute to the force-balance via viscous drag, bending, stretching, and
 139 protein friction. Viscous friction penalises relative motion between actin filaments and the
 140 background medium, giving rise to drag forces $\mathbf{F}_{a,\text{drag}}$. We account for filament bending
 141 via the variation of $E_{a,\text{bend}}$, which sums the elastic potential energy along the extent of
 142 each filament. The contribution of longitudinal spring forces, $E_{a,\text{spring}}$, follows Hooke’s law
 143 with spring constant k_a . Since actin filaments are effectively inextensible [49], we assume
 144 that k_a is large. The symbol $\mathbf{F}_{a,\text{pf}}$ represents point-wise drag due to protein friction,

145 which opposes relative motion of filament intersections. We also investigated the effect of
 146 including random filament motion due to thermal forces. These have only a small impact
 147 on stress and filament aggregation, so we neglect thermal forces in (2.1). Further details
 148 on their effects are provided in the Supporting Material.

149 The system (2.1) also contains two contributions relevant to myosin motors. Like for
 150 actin filaments, $E_{m,\text{spring}}$ is the energy associated with longitudinal spring forces. These
 151 forces are governed by Hooke’s law with the spring constant k_m , which we assume large to
 152 model the short length of myosin motors compared to actin filaments. For actin–myosin
 153 interactions we adopt a linear force–velocity relation for myosin motors, written as $\mathbf{F}_{m,a}$.
 154 Under this assumption, unloaded motors move at the velocity V_m , and that motors cannot
 155 move if force exceeds the stall force, F_s .

156 2.1 Numerical Method and Stress Calculation

157 In each simulation, we represent actin filaments as chains of nodes, with adjacent nodes
 158 connected by straight line segments. We initialise filaments as straight entities with random
 159 centre positions and orientations, such that all nodes on the same filament are equidistant.
 160 Given the initial filament network, we place myosin motors at random intersections between
 161 filaments, such that each intersection accommodates a maximum of one motor. To evolve
 162 the network, at each time step we construct and minimise the energy functional

$$163 \begin{aligned} E_{\text{net}} := & E_{a,\text{drag}} + E_{a,\text{bend}} + E_{a,\text{spring}} + E_{a,\text{pf}} \\ & + E_{m,\text{spring}} + E_{m,a}. \end{aligned} \quad (2.2)$$

164 This functional includes pseudo-energy terms $E_{a,\text{drag}}$, $E_{a,\text{pf}}$, and $E_{m,a}$, whose variations cor-
 165 respond to finite difference approximations of the force terms $\mathbf{F}_{a,\text{drag}}$, $\mathbf{F}_{a,\text{pf}}$, and $\mathbf{F}_{m,a}$, which
 166 cannot be interpreted as variations of potential energy. Further details and mathematical
 167 descriptions of the energy terms in (2.2) are provided in the Supporting Material.

168 Each time step, we use the limited-memory Broyden–Fletcher–Goldfarb–Shanno
 169 (LBFGS) method to minimise (2.2) with respect to the positions of filament nodes and
 170 myosin motors. We perform this optimisation using the `Optim.jl` [50] package in JULIA,
 171 using automatic differentiation (`ForwardDiff.jl`) to evaluate the gradient. Our energy
 172 minimisation method is time-implicit, which enables comparatively large time steps with-
 173 out loss of numerical stability. One drawback is that large time steps enable only coarse
 174 simulation of filament turnover and motor unbinding. Also, our implementation using
 175 automatic differentiation is typically slower than explicit methods.

176 A key advantage of our energy minimisation numerical method is that it enables direct
 177 computation of the forces on the domain boundary required to prevent uniform elongation

178 and shear deformations. These forces aggregate the contributions of each filament and
 179 motor in the network, and thus provide a measure of contractility. We compute these
 180 forces, \mathbf{F}_x and \mathbf{F}_y , by adding extra terms to the energy functional, and defining the total
 181 energy

$$182 \quad E_{\text{total}} := E_{\text{net}} + \mathbf{F}_x \cdot \mathbf{L}_x + \mathbf{F}_y \cdot \mathbf{L}_y, \quad (2.3)$$

183 where $\mathbf{L}_x = (L_{xx}, L_{xy})^T$ and $\mathbf{L}_y = (L_{yx}, L_{yy})^T$ are vectors representing two edges of the
 184 domain. The vectors $\mathbf{F}_x = (F_{xx}, F_{xy})^T$ and $\mathbf{F}_y = (F_{yx}, F_{yy})^T$, illustrated in Figure 2,
 185 contain the normal and shear forces acting on the domain boundaries.

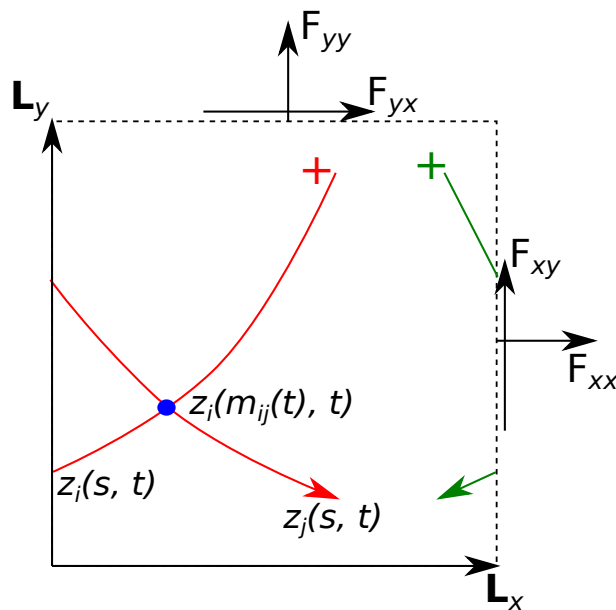


Figure 2: Schematic diagram of the periodic domain, two actin filaments, and a myosin motor. The vectors $z_i(s, t) \in \mathbb{R}^2$ denote filament positions, parameterised by the arc length s . The variable $m_{ij}(t)$ is the position of the motor.

186 In practice, we simulate the model on a two-dimensional domain of fixed geometry,
 187 keeping the vectors \mathbf{L}_x and \mathbf{L}_y constant. Minimising (2.2) is then equivalent to minimising
 188 (2.3), where the normal and shear force components are Lagrange multipliers that constrain
 189 the domain to constant size and shape. In numerical simulations, we solve the model using
 190 (2.2), then compute $\mathbf{F}_x = -\partial_{\mathbf{L}_x} E_{\text{net}}$ and $\mathbf{F}_y = -\partial_{\mathbf{L}_y} E_{\text{net}}$ using automatic differentiation.
 191 After calculating \mathbf{F}_x and \mathbf{F}_y , we combine the force components to compute the two-
 192 dimensional plane stress tensor,

$$193 \quad \boldsymbol{\sigma} = \begin{bmatrix} F_{xx}/L_{yy} & F_{xy}/L_{yy} \\ F_{yx}/L_{xx} & F_{yy}/L_{xx} \end{bmatrix}. \quad (2.4)$$

194 This describes the state of stress in the network at any time step, neglecting out-of-plane
 195 stresses. Although in-plane shear can produce non-zero out-of-plane normal stress [51,

196 52], we anticipate that out-of-plane terms will be small compared to in-plane normal
 197 stresses. To obtain a measure of contractility in a simulation, we define the bulk stress
 198 and time-averaged bulk stress

$$199 \quad \sigma = \frac{1}{2} \text{tr}(\boldsymbol{\sigma}), \quad \text{and} \quad \bar{\sigma} = \frac{1}{T} \int_0^T \sigma \, dt \quad (2.5)$$

200 respectively, where T is the time over which the simulation runs, and $\text{tr}(\boldsymbol{\sigma})$ is the trace
 201 of the stress tensor, which is invariant to co-ordinate rotations. The trace is also equal
 202 to the sum of the eigenvalues of $\boldsymbol{\sigma}$, and the associated eigenvectors indicate the principal
 203 stress directions. By convention, negative $\bar{\sigma}$ indicates contraction, and positive $\bar{\sigma}$ indicates
 204 expansion. Our method of quantifying network stress enables addition or removal of
 205 features from the energy functional, without changing the method of computing the forces.
 206 This flexibility is another advantage of our approach. In addition, our framework enables
 207 explicit simulation of domain deformation, by treating \mathbf{F}_x and \mathbf{F}_y as applied external
 208 forces instead of Lagrange multipliers, and \mathbf{L}_x and \mathbf{L}_y as degrees of freedom. Contractile
 209 networks would then cause $|\mathbf{L}_x|$ and $|\mathbf{L}_y|$ to decrease, and expansive networks would cause
 210 $|\mathbf{L}_x|$ and $|\mathbf{L}_y|$ to increase.

211 3 Results and Discussion

212 We use numerical simulations of our mathematical model to investigate how filament
 213 bending and protein friction affect contractility. In general, we simulate actomyosin
 214 networks using a default set of biophysically-realistic parameters obtained from literature
 215 [18, 27, 42, 44, 48, 53–66]. The complete list of parameter values and details on their
 216 estimation are provided in the Supporting Material. We outline the main simulation
 217 results under subsequent headings.

218 3.1 Actin Filament Bending Facilitates Network Contraction

219 To investigate actin filament bending as a contractile mechanism, we compared 25 simula-
 220 tions of semi-flexible filaments with 25 simulations of rigid, straight filaments. In each
 221 simulation, we simulated 50 filaments and 10 motors in a domain of width $2.5 \mu\text{m}$, and ran
 222 simulations until $T = 60 \text{ s}$, with a time step size of $\Delta t = 0.05 \text{ s}$. This is sufficient to obtain
 223 results independent of the domain width and time step size (see Supporting Material).
 224 We then compared the time-averaged bulk stresses (2.5), and these reveal that bending is
 225 essential for contraction. As panel A of Figure 3 shows, the network contracted in each
 226 simulation with semi-flexible filaments (mean $\bar{\sigma} = -0.072 \text{ pN } \mu\text{m}^{-1}$), but always expanded
 227 with rigid filaments (mean $\bar{\sigma} = 0.161 \text{ pN } \mu\text{m}^{-1}$). With rigid filaments, we observe net

228 expansion because motor movement biases mean motor position towards filament plus-ends.
 229 In subsequent results (see Figure 4), we will show this to be an expansive configuration.
 230 However, filament bending counteracts this tendency to expand, facilitating systematic
 231 bias to contraction.

232 We hypothesise that the magnitude of contraction depends on the extent of filament
 233 bending in the network. To investigate this, at each time step in the simulations we
 234 compute the local curvature

$$235 \quad \kappa(s) = \sqrt{x''(s)^2 + y''(s)^2} \quad (3.1)$$

236 at each filament node. To obtain a measure of total curvature for one filament, we use the
 237 trapezoidal rule to integrate the curvature along the filament. We quantify the extent of
 238 filament bending in the network by averaging the integrated curvature over all filaments
 239 and time, defining

$$240 \quad \bar{\kappa} = \frac{1}{T} \frac{1}{N_a} \sum_{i=1}^{N_a} \int_0^T \int_0^{L_i} \kappa(s) \, ds \, dt. \quad (3.2)$$

241 In the remainder of this manuscript, bar notation will represent quantities similarly
 242 averaged over filaments and time.

243 Since the flexural rigidity describes the resistance of a filament to bending, we varied
 244 κ_a and investigated its effect on stress production. For each value of κ_a tested, we ran
 245 ten random simulations and computed $\bar{\sigma}$. Box plots of network bulk stress presented in
 246 panel B of Figure 3 show that decreasing κ_a increases contractility. This is expected,
 247 because decreased values of κ_a correspond to decreased resistance to filament bending. As
 248 panel C of Figure 3 shows, the increase in contractile stress that occurs with decreasing
 249 κ_a corresponds to increased filament curvature. This accords with the hypothesis that
 250 filament bending gives rise to force asymmetry, and subsequently contraction. Furthermore,
 251 the flexural rigidity for actin filaments, $\kappa_a = 0.073 \text{ pN } \mu\text{m}^2$ [53], lies within the region for
 252 which we expect contraction. Actin filament bending is thus a plausible mechanism of
 253 contraction in biological cells.

254 3.2 Bending Facilitates Net Contraction on the Microscopic Scale

255 To better understand the microscopic mechanisms of contraction, we simulate assemblies
 256 of two actin filaments with an attached myosin motor. Our objective is to determine
 257 whether the force asymmetry occurs in this simple structure, or whether contraction relies
 258 on network-scale interactions. In two-filament simulations, we use $\lambda_a = 10 \text{ pN } \mu\text{m}^{-2} \text{ s}$,
 259 which is larger than the value $\lambda_a = 0.05 \text{ pN } \mu\text{m}^{-2} \text{ s}$, used in network simulations. This
 260 is because we assume the two-filament structure is embedded in a dense, homogeneous

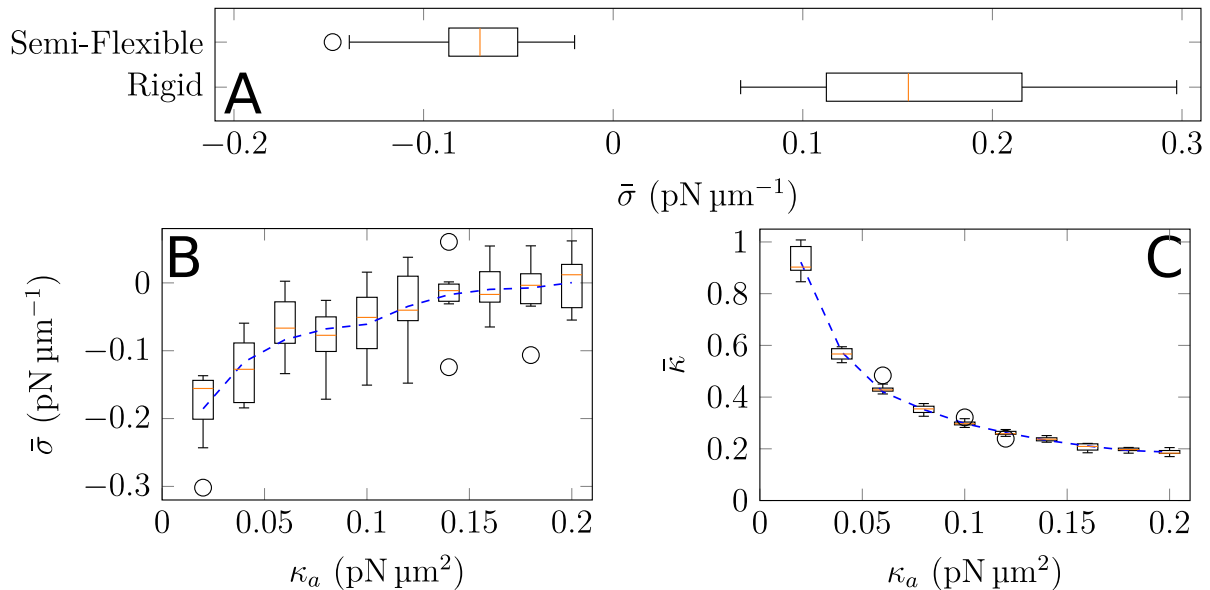


Figure 3: (A): Box plots comparing mean $\bar{\sigma}$ in ten semi-flexible networks and ten rigid networks. (B–C): The effect of flexural rigidity, κ_a , on (B) $\bar{\sigma}$ and (C) $\bar{\kappa}$. Box plots represent data from ten simulations with a given parameter, and the dashed curve is mean data smoothed with a Savitsky–Golay filter.

261 background network. When a single fibre is immersed in such a network, protein friction
 262 manifests itself as drag acting uniformly along the entire filament length. The larger value
 263 of λ_a then replaces protein friction at filament intersections, which cannot occur in the
 264 two-filament simulations because the motor occupies the only intersection.

265 We initialise the two filaments in a square domain, and characterise their positions
 266 by the angle $\theta \in [0, \pi]$, which is the angle between the two filaments measured at their
 267 intersection point. The relative motor positions are denoted by m_1 and m_2 , such that
 268 $m_i \in [0, L_i]$ for $i = 1, 2$, measures the distance of the motor binding site from the minus
 269 end of filament i . We hypothesise that the extent of expansion or contraction of the
 270 two-filament structure depends on θ , m_1 , and m_2 . As the motor slides the filaments, it
 271 pulls filament branches between the motor and plus-ends together, generating contraction.
 272 Simultaneously, it pushes filament branches between the motor and minus-ends apart,
 273 generating expansion. Furthermore, the filaments will move the most if they are anti-
 274 parallel, or $\theta = \pi$. Conversely, when filaments are parallel ($\theta = 0$), the motor will traverse
 275 the filaments without generating relative motion.

276 Panels A–J of Figure 4 illustrate two-filament simulations for both rigid and semi-
 277 flexible filaments. In the upper row (A–E), the rigid filaments evolve symmetrically. As the
 278 motor traverses the filaments from the minus to plus ends, the filaments move and rotate
 279 such that their final position is a mirror image of the original. As reported by Lenz [9],
 280 this polarity-reversal symmetry causes the initial contraction and subsequent expansion

281 to cancel. Principal stress arrows in the upper panel confirm this. The result is no net
 282 contraction for rigid filaments. However, the picture is different for semi-flexible filaments,
 283 as the lower row (F–J) reveals. When the motor begins to move, filament bending increases
 284 θ , increasing contraction in the x -direction. Subsequently, as the motor positions become
 285 favourable to expansion the angle between the filaments decreases (see the fourth image in
 286 the lower panel), decreasing the magnitude of expansion. Consequently, the semi-flexible
 287 filaments experience net contraction, providing evidence of the force asymmetry.

288 To verify this, we plot the bulk stress and θ versus time, for both rigid and semi-flexible
 289 filaments. The bulk stress results in panel K of Figure 4 confirm that rigid filaments
 290 experience no net contraction, because the magnitude of early contraction is equal to the
 291 magnitude of later expansion. The results in panel L of Figure 4 support this, where
 292 the angle θ for the initial contraction mirrors the angle for the subsequent expansion.
 293 In contrast, for semi-flexible filaments the structure experiences larger contractile than
 294 expansive stress. This is because filament bending **leads to** an asymmetric pattern in
 295 θ with time, with a decrease as the motor approaches the plus ends. As a result, the
 296 semi-flexible filaments are unable to attain the large expansion that occurs towards the
 297 end of the rigid filament solution. This analysis confirms that a force asymmetry is a
 298 possible explanation for bending-induced actomyosin contraction.

299 **3.3 A Heuristic Index Predicts Stress Generated By Two-Filament-** 300 **Motor Assemblies**

301 Inspired by the previous results on the contraction of a two-filament-motor assembly, we
 302 propose a heuristic index that summarises the contractile potential of two filaments,

$$303 \quad I_2 = \left[\frac{2(m_1 + m_2)}{L_1 + L_2} - 1 \right] \sin^2 \left(\frac{\theta}{2} \right). \quad (3.3)$$

304 In (3.3), the left term in the brackets describes the length of the expansive and contractile
 305 branches, such that it is -1 if both motors are at the minus ends (contractile), and 1 if
 306 both motors are at the plus ends (expansive). To capture the effect of angle, the term in
 307 the right brackets is zero if $\theta = 0$, and 1 if $\theta = \pi$.

308 To confirm the effect of angle on contraction, we plot I_2 (3.3) versus time in the
 309 two-filament simulations. In panels M–N of Figure 4, we multiplied I_2 by a constant
 310 such that its minimum is equal to the minimum stress obtained in the simulation. **We**
 311 **refer to this normalised index as \tilde{I}_2** . The index accurately predicts the bulk stress in
 312 both simulations. Of particular note, \tilde{I}_2 correctly predicts the loss of contraction with
 313 semi-flexible filaments, as panel N of Figure 4 shows. Combined with panel L of Figure 4,

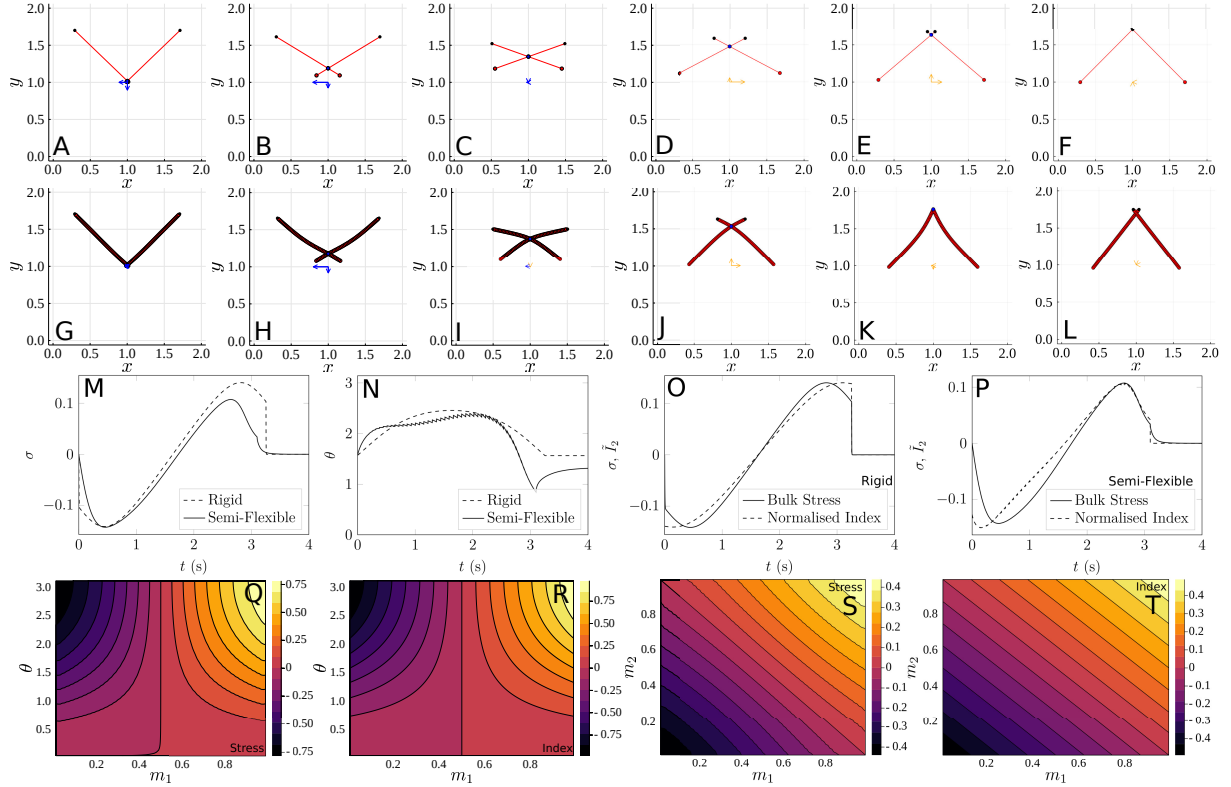


Figure 4: (A–F): Two-filament simulations with initial motor positions $m_1 = m_2 = 0$, and $\theta = \pi/2$. (A–F): rigid actin filaments, (G–L): Semi-flexible filaments. Results are presented (left–right) at $t \in \{0.04, 0.5, 1.55, 2.59, 3.09, 4\}$ s. Arrows centred at (1, 1) indicate the principal stress directions, and their lengths (given by the eigenvalues of $\boldsymbol{\sigma}$) represent the relative magnitude of stress. Blue arrows represent contraction, orange arrows represent expansion. (M–N): σ and θ versus time in two-filament simulations. (O–P): Comparison of σ and \tilde{I}_2 in rigid and semi-flexible two-filament simulations. (Q–T): Comparison between σ and I_2 for one time step of a two-filament simulation, with $\Delta t = 2 \times 10^{-5}$ s.

314 this shows that filament bending **facilitates** contraction by influencing the angle between
 315 filaments, such that larger angles occur under contraction than under expansion.

316 To confirm the predictive ability of (3.3), we compute I_2 for varying m_1 , m_2 , and θ .
 317 For each configuration, we compute one time step and compare the simulated bulk stress
 318 with (3.3). The results in panels O–R of Figure 4 show that the two-filament index I_2
 319 effectively captures the stress generated by two filaments. This is true if we hold $m_1 = m_2$
 320 and vary θ (as in panels O–P), and if we hold θ constant and vary both m_1 and m_2 (as in
 321 panels Q–R).

322 3.4 Protein Friction Enables Network-Scale Contraction

323 Protein friction, either from cross-linking or filament contact, penalises relative motion
 324 where filaments overlap. Previous studies have suggested that intermediate cross-linker
 325 density maximises contraction [25, 29, 31, 41, 67, 68]. Without cross-linking, filaments
 326 move independently of each other, and are unable to generate collective contraction.
 327 However, strongly cross-linked networks generate large resistance to filament motion as
 328 myosin moves, which also inhibits contraction. To investigate this dependence using our
 329 model, we varied the protein friction drag coefficient, λ_{pf} , and computed ten simulations
 with each parameter value. Results from these simulations are shown in Figure 5.

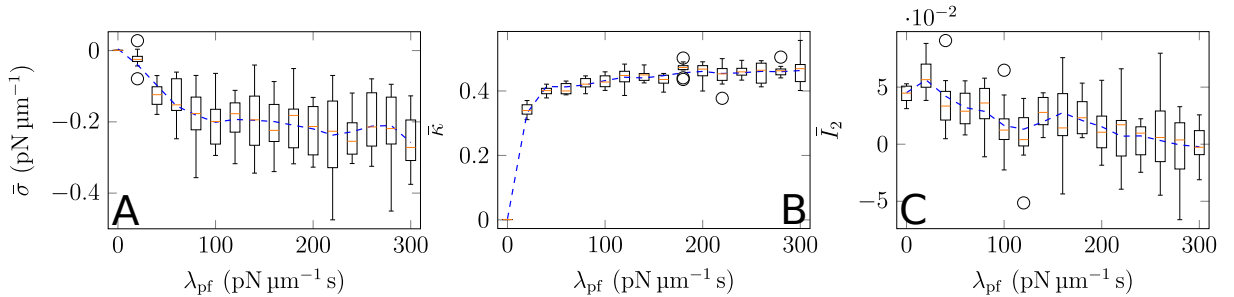


Figure 5: The effect of protein friction coefficient, λ_{pf} , on (A) $\bar{\sigma}$, (B) $\bar{\kappa}$, and (C) \bar{I}_2 . Box plots represent data from ten simulations with a given parameter, and the dashed curve is mean data smoothed with a Savitsky–Golay filter.

330
 331 Panel A of Figure 5 shows the relationship between λ_{pf} and bulk stress. As expected,
 332 networks become more contractile as λ_{pf} increases from zero. Although the precise
 333 value of the protein friction coefficient for actin filaments is unknown, Ward et al. [48]
 334 suggests protein friction due to filament contact of approximately $\lambda_{\text{pf}} = 30$ pN μm^{-1} s.
 335 Estimating λ_{pf} based on the cross-linker α -actinin yields approximately $\lambda_{\text{pf}} = 20$ pN μm^{-1} s
 336 (see Supporting Material). Both values are sufficient to demonstrate contractile bias.
 337 Subsequent increases in λ_{pf} beyond these values incur diminishing returns, such that
 338 contractility becomes stable after approximately $\lambda_{\text{pf}} = 200$ pN μm^{-1} s. We do not observe a

339 U-shaped curve in stress with λ_{pf} . A possible explanation is the sparseness of our simulated
340 networks, which does not enable sufficient connectivity to restrict contraction, given that
341 we assume no protein friction between filament pairs with a motor attached.

342 Plots of the time-averaged curvature and I_2 in panels B–C of Figure 5 respectively
343 demonstrate that contraction correlates with increased curvature and decreased I_2 . An
344 important finding is that filament bending does not occur in the absence of protein friction.
345 This is because protein friction supplies resistance to motion at specific points along
346 the filament. Without this drag, neglecting thermal fluctuations the filament will tend
347 to adopt the energetically-preferable straight configuration. Therefore, protein friction
348 is essential to contraction. Furthermore, only a small increase in filament bending is
349 attainable by increasing the protein friction coefficient beyond the biologically-feasible
350 value of $\lambda_{\text{pf}} = 30 \text{ pN } \mu\text{m}^{-1} \text{ s}$.

351 **3.5 Viscous Friction Inhibits Contraction**

352 The viscous drag coefficient λ_a represents drag between actin filaments and structures
353 external to the network. This can arise from drag between the filaments and the cytoplasm,
354 or drag between filaments and a dense, homogeneous background network that interacts
355 uniformly with the simulated filaments. Increasing λ_a thus corresponds to increasing
356 cytoplasm viscosity, or increasing the network density. *In vitro* experiments by Murrell
357 and Gardel [16] showed that increasing adhesion between actomyosin networks and the
358 membrane inhibits contraction. We suggest that increased membrane adhesion corresponds
359 to an increase in drag coefficient in our model, because both restrict filament motion. For
360 these reasons, we are interested in how contractility depends on λ_a .

361 We varied λ_a and performed ten simulations for each parameter value. These results are
362 shown in panel A of Figure 6. As predicted by experiments, network contractility increases
363 as we decrease λ_a . Interestingly, panels B–C of Figure 6 show that this increased contraction
364 does not correspond to an increase in filament curvature or decrease in the two-filament
365 index. Instead, a possible explanation is that increasing λ_a increases resistance to actin
366 filament movement. When myosin motors exert forces on the network, a larger proportion
367 is used to overcome drag as λ_a increases. This inhibits the ability of myosin motors to
368 remodel the network, and this slower remodelling results in decreased contraction.

369 **3.6 Myosin Unbinding Does Not Affect the Mechanism of Contraction**

371 Myosin motor unbinding is another feature of our model that might influence contractility.
372 In our simulations, motor unbinding is governed by Bell’s law. All motors that have not

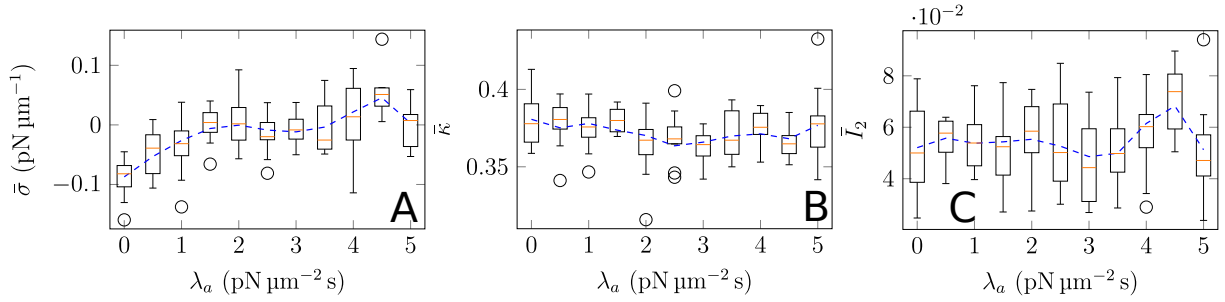


Figure 6: The effect of viscous drag coefficient, λ_a , on (A) $\bar{\sigma}$, (B) $\bar{\kappa}$, and (C) \bar{I}_2 . Box plots represent data from ten simulations with a given parameter, and the dashed curve is mean data smoothed with a Savitsky–Golay filter.

373 reached the end of a filament unbind with a rate that depends on the spring force on the
 374 motor, and the reference off-rate, $k_{\text{off},m}$. To investigate how this off-rate affects contractility,
 375 we computed a series of simulations with varying $k_{\text{off},m}$, and present results in panels A–C
 376 of Figure 7.

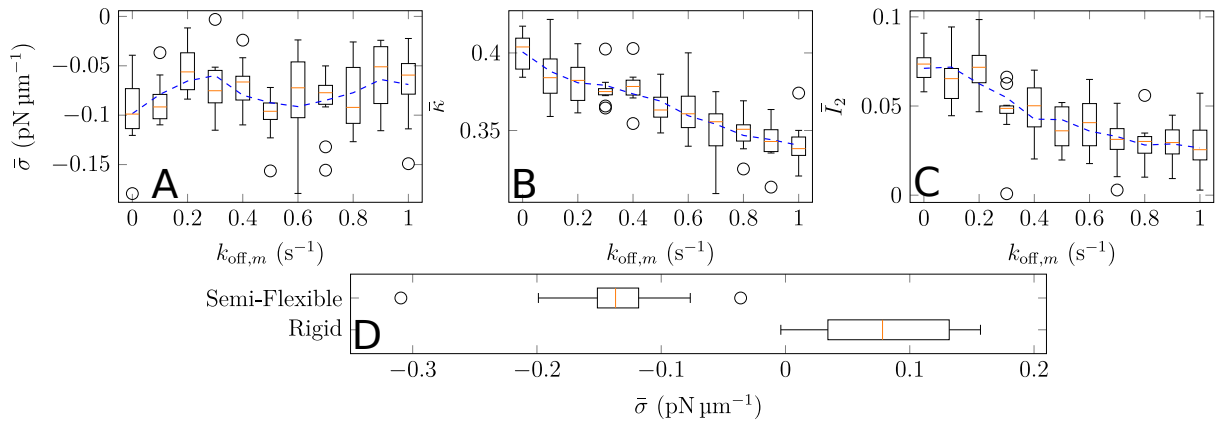


Figure 7: (A–C): The effect of reference motor off-rate, $k_{\text{off},m}$, on (A) $\bar{\sigma}$, (B) $\bar{\kappa}$, and (C) \bar{I}_2 . Box plots represent data from ten simulations with a given parameter, and the dashed curve is mean data smoothed with a Savitsky–Golay filter. (D): Box plots comparing mean $\bar{\sigma}$ in 25 semi-flexible networks and 25 rigid networks, with force-independent motor unbinding.

377 Overall, the reference off-rate has no consistent effect on stress. However, panels B–C
 378 of Figure 7 suggest that the means of contraction changes as $k_{\text{off},m}$ changes. A possible
 379 explanation is that $k_{\text{off},m}$ governs the expected time for which a motor remains attached
 380 to the filaments. For example, lower values of $k_{\text{off},m}$ enable motors to remain attached
 381 to actin filaments for longer time. Highly-persistent motors have longer time to initiate
 382 bending, and therefore curvature increases as $k_{\text{off},m}$ decreases (see panel B). However, such
 383 persistent motors also walk further towards the plus ends, increasing I_2 (see panel C). As
 384 previously shown, motor positioning closer to the plus ends is favourable for expansion.
 385 The competing effects of filament bending and motor position enable disordered networks

386 to generate similar contractile stress for all reference motor off-rates tested.

387 We also tested **how** the force-dependence introduced by Bell’s law influences con-
388 tractility. To do this, we performed **25** simulations with both rigid and semi-flexible
389 filaments, and compare the time-averaged bulk stress results with the default simulations
390 in panel A of Figure 3. Results with force-independent unbinding are given in panel D
391 of Figure 7. **Compared to simulations with force-dependent unbinding, simulations with**
392 **force-independent unbinding display a small bias to contraction in both rigid and semi-**
393 **flexible simulations. A possible explanation is that the stretching force on a myosin motor**
394 **is larger for anti-parallel filament assemblies undergoing contraction. With force-dependent**
395 **unbinding, motors more readily unbind from these anti-parallel assemblies, decreasing**
396 **contractility. However, since the results in Figure 7, panel D, are similar to Figure 3, panel**
397 **A, this does not affect the mechanism of contraction.**

398 **3.7 Actin Filament Turnover Enables Persistent Contraction**

399 In biological cells, actin filament turnover is an important process that enables sustained
400 contraction. Turnover refers to the exchange of proteins with the background cytoplasm,
401 and introduces randomness. Without turnover, actomyosin networks have been shown
402 to lose contractility over time [7, 12, 17, 27, 41, 45]. To investigate whether our model
403 replicates this behaviour, we varied the actin filament turnover rate, $k_{\text{off},a}$, and present
404 results for the simulated stress in panel A of Figure 8. Time-averaged stress results
405 show increased contraction as we increase actin turnover rate. In support of this, panels
406 B–C of Figure 8 show that increased actin turnover corresponds to a decrease in mean
407 integrated filament curvature, and the two-filament index shows bias towards expansive
408 configurations.

409 To investigate the time-dependence of contractile stress with and without turnover, we
410 plot the mean bulk stress in the ten simulations versus time for $k_{\text{off},a} = 0 \text{ s}^{-1}$ (no turnover)
411 and $k_{\text{off},a} = 0.2 \text{ s}^{-1}$ (fast turnover). With no turnover, there is a loss of contractility as
412 time progresses (see panel D), whereas no trend occurs with fast turnover. Since both
413 networks in panels D–E of Figure 8 show similar contractile stress at $t = 0$, the results in
414 panel A of Figure 8 occur because the network loses contractility if there is no turnover,
415 decreasing time-averaged stress $\bar{\sigma}$.

416 Previous studies have shown that loss of contraction in the absence of turnover is
417 associated with pattern formation in the network. This involves filaments aggregating
418 in asters [69] or bundles [70], after which they do not move under molecular motor
419 activity. To investigate whether **filament aggregation** occurs in our simulations, we
420 computed the distance between all pairs of nodes on different filaments. If the distribution
421 of these distances differs from the expected distribution for two random points in a

422 square, we conclude that filaments have aggregated. An example comparison of these
 423 distance distributions at 300 s, and the corresponding network images, are provided in
 424 panels F–I of Figure 8. With no turnover, there are two peaks in the distribution of
 425 distances that are not predicted by the theoretical distribution. In contrast, the distance
 426 distribution closely matches the theoretical distribution in the simulation with fast turnover,
 427 $k_{\text{off},a} = 0.2 \text{ s}^{-1}$. This provides evidence that actin filaments aggregate with no turnover.
 428 Fast turnover prevents this **filament aggregation** by introducing randomness to filament
 429 positions, enabling persistent contraction. Similar distributions occur across all simulations,
 a complete summary of which is given in the Supporting Material.

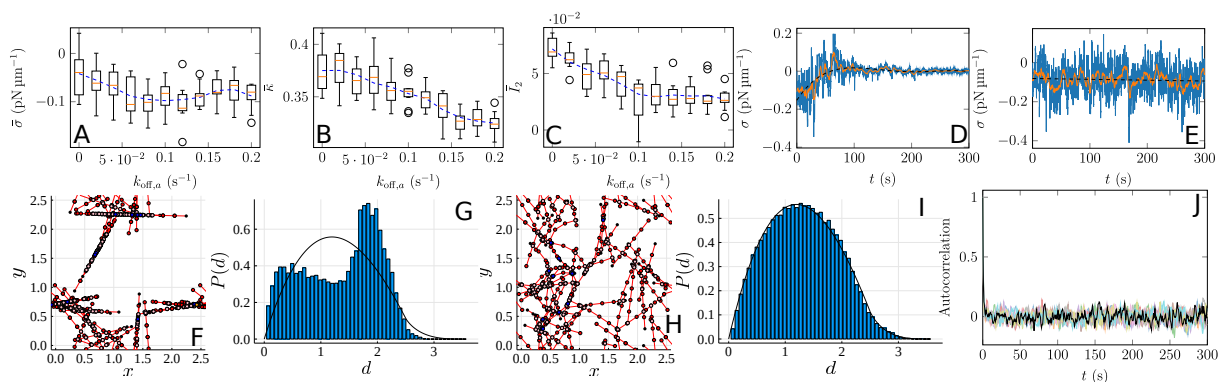


Figure 8: (A–C): The effect of actin turnover rate, $k_{\text{off},a}$, on (A) $\bar{\sigma}$, (B) $\bar{\kappa}$, and (C) \bar{F}_z . Box plots represent data from ten simulations with a given parameter, and the dashed curve is mean data smoothed with a Savitsky–Golay filter. (D–E): Mean bulk stress (blue curve) for ten simulations versus time, with (D) $k_{\text{off},a} = 0 \text{ s}^{-1}$, and (E) $k_{\text{off},a} = 0.2 \text{ s}^{-1}$. The orange curve is a moving average with window width 10 s, and the dashed curve is a fit to mean data. (F–I): Network configurations and distributions of the distances between pairs of actin filament nodes in the network at $t = 300 \text{ s}$. Blue bars represent simulation results, and the black curve is the theoretical distribution for the distance between two random points in a square [71]. (F–G): No turnover, $k_{\text{off},a} = 0 \text{ s}^{-1}$. (H–I): Fast turnover, $k_{\text{off},a} = 0.2 \text{ s}^{-1}$. (J): Autocorrelation function of the stress σ . **The transparent curves represent ten individual simulations, and the opaque black curve is the autocorrelation of the mean stress.**

430

431 3.8 Simulated Networks Do Not Exhibit Periodic Pulsation

432 Interestingly, periodic or pulsed contraction has been observed in experiments and simula-
 433 tions with filament turnover [17, 41, 72, 73]. Some authors have suggested that biochemical
 434 signals external to the network are responsible for this pulsation [72, 73]. However, recent
 435 work by Yu et al. [74] showed that pulsation might be an inherent result of actomyosin
 436 mechanics, caused by actin treadmilling or severing. As panels D–E of Figure 8 show, stress
 437 rises and falls in our simulations with or without turnover, indicating pulse-like behaviour.

438 To investigate whether solutions with turnover have a characteristic period of pulsation,
439 we simulated 10 random networks to $T = 600$ s, with default parameters. Plotting the
440 autocorrelation of the stress signal then enables us to determine whether a characteristic
441 period exists. These results are shown in panel J of Figure 8. Autocorrelation compares
442 original stress signal and a time-delayed version, and returns the correlation coefficient at
443 a function of the time delay. If stress generation is periodic with period T , we would see
444 peaks in the autocorrelation at all multiples of T . In panel J of Figure 8, no such peaks
445 appear in the first five minutes of the ten solutions or mean data. Therefore, although our
446 results show oscillations in contractile stress, these oscillations are aperiodic.

447 Our findings extend the results of Belmonte, Leptin, and Nédélec [17], who used
448 visual inspection of simulations to show that pulsation occurs in networks with turnover.
449 Our results are consistent with observations that pulsation occurs due to biochemically-
450 regulated, periodic formation of actomyosin networks [72, 73], and not necessarily periodic
451 stress generation within the networks. Observing periodic mechanical behaviour would
452 require additional features to those in our model. Examples might include actin treadmilling
453 or severing, which Yu et al. [74] showed to be necessary for pulsed contraction in the
454 absence of biochemical regulation.

455 4 Conclusion

456 Contraction of disordered actomyosin networks is essential to biological cell function. Since
457 the origins of this contraction are not yet fully understood, scientists have worked to
458 build an inventory of possible contraction mechanisms. In this study, we investigated
459 the hypothesis that protein friction, arising from cross-linking or solid friction between
460 actin filaments, enables contraction of networks consisting of semi-flexible actin filaments.
461 We achieved this by developing an agent-based mathematical model for two-dimensional
462 actomyosin networks. By formulating the force-balance equations as a gradient flow, our
463 model provides a way of quantifying network stress. Numerical simulations confirmed that
464 actin filament bending facilitates a force asymmetry that biases contraction over expansion
465 in random networks. Importantly, network-scale bending is only possible with protein
466 friction, making protein friction crucial to contraction.

467 To understand the bending-induced force asymmetry at the microscopic scale, we
468 simulated the simplest actomyosin assembly consisting of a single myosin motor bound
469 to two actin filaments. For both rigid and semi-flexible filaments, the contractile force
470 depends on the motor relative positions, and the angle between the two filaments. As the
471 motor moves from the minus to the plus ends, semi-flexible filaments generate a wider
472 angle than rigid filaments. Since these wider angles are more conducive to contraction,

473 our microscopic simulations showed that filament bending induces contractile bias at
474 the microscopic scale. Furthermore, this confirmed that bending forces are sufficient to
475 facilitate contraction.

476 Our simulations also confirmed previous experimental and theoretical results that
477 filament turnover is required to sustain contraction. Although actin bending and protein
478 friction facilitate contraction, without turnover the filaments aggregate and form patterns,
479 after which the network loses contractility. In our simulations, introducing turnover
480 causes a more random spatial distribution of filaments, and enables the network to sustain
481 contractility. However, in many cell types actin filaments can form contractile actomyosin
482 bundles such as stress fibres, which are aggregated structures that sustain and mediate
483 contractility [75]. An important application of our modelling and simulation framework
484 will be to identify the minimal mechanisms that enable self-organisation and persistence
485 of such bundles, even in networks with fast turnover. We plan to tackle this problem in
486 future work.

487 Finally, our theoretical predictions could be tested using *in vitro* actomyosin assays.
488 One testable prediction is the detailed dependence of stress on filament flexural rigidity
489 (Figure 3, panel B). This could be tested using actomyosin assays similar to Alvarado
490 et al. [76], by comparing experimental measurements of force or contraction with our stress
491 results. Another testable prediction is the dependence of the protein friction coefficient on
492 stress (Figure 5, panel A). This could be tested by varying the concentration of cross-linkers,
493 which governs λ_{pf} according to the formula in the Supporting Material. Furthermore,
494 results from *in vitro* assays could be compared with our predictions of the effect of actin
495 filament turnover rate on stress (Figure 8, panel A). Computing a pair-correlation function
496 to mimic the distance distributions visualised in panels G and I of Figure 8, would also
497 enable comparison with the quantitative predictions on aggregation reported in more
498 detail in the Supporting Material. Overall, experimental validation could uncover whether
499 the minimal mechanics included in our model is sufficient. If not, possible extensions to
500 the model include simulating filament polymerisation or treadmilling, three-dimensional
501 description of the material mechanics [52], or consideration of odd elasticity [77].

502 **5 Author Contributions**

503 A. K. Y. T. and D. B. O. designed the research and developed the mathematical model.
504 A. K. Y. T. performed the numerical simulations, analysed the data, and wrote the
505 manuscript, with guidance from D. B. O and A. M.

6 Acknowledgements

The authors acknowledge funding from the Australian Research Council (ARC) Discovery Program (grant number DP180102956), awarded to D. B. O. and A. M.

References

- [1] M. Gautel, “The sarcomeric cytoskeleton: who picks up the strain?”, *Current Opinion in Cell Biology* 23 (2011), pp. 39–46, DOI: [10.1016/j.ceb.2010.12.001](https://doi.org/10.1016/j.ceb.2010.12.001).
- [2] T. D. Pollard, “Mechanics of cytokinesis in eukaryotes”, *Current Opinion in Cell Biology* 22 (2010), pp. 50–56, DOI: [10.1016/j.ceb.2009.11.010](https://doi.org/10.1016/j.ceb.2009.11.010).
- [3] K. M. Yamada and M. Sixt, “Mechanisms of 3D cell migration”, *Nature Reviews Molecular Cell Biology* 20 (2019), pp. 738–752, DOI: [10.1038/s41580-019-0172-9](https://doi.org/10.1038/s41580-019-0172-9).
- [4] K. J. Chalut and E. K. Paluch, “The actin cortex: a bridge between cell shape and function”, *Developmental Cell* 38 (2016), pp. 571–573, DOI: [10.1016/j.devcel.2016.09.011](https://doi.org/10.1016/j.devcel.2016.09.011).
- [5] T. D. Pollard, “The value of mechanistic biophysical information for systems-level understanding of complex biological processes such as cytokinesis”, *Biophysical Journal* 107 (2014), pp. 2499–2507, DOI: [10.1016/j.bpj.2014.10.031](https://doi.org/10.1016/j.bpj.2014.10.031).
- [6] T. H. Cheffings, N. J. Burroughs, and M. K. Balasubramanian, “Actomyosin ring formation and tension generation in eukaryotic cytokinesis”, *Current Biology* 26 (2016), R719–R739, DOI: [10.1016/j.cub.2016.06.071](https://doi.org/10.1016/j.cub.2016.06.071).
- [7] B. Y. Rubinstein and A. Mogilner, “Myosin clusters of finite size develop contractile stress in 1D random actin arrays”, *Biophysical Journal* 113 (2017), pp. 937–947, DOI: [10.1016/j.bpj.2017.07.003](https://doi.org/10.1016/j.bpj.2017.07.003).
- [8] D. Gordon, A. Bernheim-Groswasser, C. Keasar, and O. Farago, “Hierarchical self-organization of cytoskeletal active networks”, *Physical Biology* 9, 026005 (2012), DOI: [10.1088/1478-3975/9/2/026005](https://doi.org/10.1088/1478-3975/9/2/026005).
- [9] M. Lenz, “Geometrical origins of contractility in disordered actomyosin networks”, *Physical Review X* 4, 041002 (2014), DOI: [10.1103/PhysRevX.4.041002](https://doi.org/10.1103/PhysRevX.4.041002).
- [10] T. Hiraiwa and G. Salbreux, “Role of turnover in active stress generation in a filament network”, *Physical Review Letters* 116, 188101 (2016), DOI: [10.1103/PhysRevLett.116.188101](https://doi.org/10.1103/PhysRevLett.116.188101).
- [11] A. E. Carlsson, “Contractile stress generation by actomyosin gels”, *Physical Review E* 74, 051912 (2006), DOI: [10.1103/PhysRevE.74.051912](https://doi.org/10.1103/PhysRevE.74.051912).

- 538 [12] D. B. Oelz, B. Y. Rubinstein, and A. Mogilner, “A combination of actin treadmilling
539 and cross-linking drives contraction of random actomyosin arrays”, *Biophysical*
540 *Journal* 109 (2015), pp. 1818–1829, DOI: [10.1016/j.bpj.2015.09.013](https://doi.org/10.1016/j.bpj.2015.09.013).
- 541 [13] K. Kruse and F. Jülicher, “Actively contracting bundles of polar filaments”, *Physical*
542 *Review Letters* 85 (2000), pp. 1778–1781, DOI: [10.1103/PhysRevLett.85.1778](https://doi.org/10.1103/PhysRevLett.85.1778).
- 543 [14] M. Lenz, M. L. Gardel, and A. R. Dinner, “Requirements for contractility in dis-
544 ordered cytoskeletal bundles”, *New Journal of Physics* 14, 033037 (2012), DOI:
545 [10.1088/1367-2630/14/3/033037](https://doi.org/10.1088/1367-2630/14/3/033037).
- 546 [15] V. Wollrab, J. M. Belmonte, L. Baldauf, M. Leptin, F. Nédélec, and G. H. Koenderink,
547 “Polarity sorting drives remodeling of actin-myosin networks”, *Journal of Cell Science*
548 132, jcs219717 (2019), DOI: [10.1242/jcs.219717](https://doi.org/10.1242/jcs.219717).
- 549 [16] M. P. Murrell and M. L. Gardel, “F-actin buckling coordinates contractility and
550 severing in biomimetic actomyosin cortex”, *Proceedings of the National Academy*
551 *of Science of the United States of America* 109 (2012), pp. 20820–20825, DOI: [10.](https://doi.org/10.1073/pnas.1214753109)
552 [1073/pnas.1214753109](https://doi.org/10.1073/pnas.1214753109).
- 553 [17] J. M. Belmonte, M. Leptin, and F. J. Nédélec, “A theory that predicts behaviors of
554 disordered cytoskeletal networks”, *Molecular Systems Biology* 13, 941 (2017), DOI:
555 [10.15252/msb.20177796](https://doi.org/10.15252/msb.20177796).
- 556 [18] T. Kamasaki, M. Osumi, and I. Mabuchi, “Three-dimensional arrangement of F-
557 actin in the contractile ring of fission yeast”, *Journal of Cell Biology* 178 (2007),
558 pp. 765–771, DOI: [10.1083/jcb.200612018](https://doi.org/10.1083/jcb.200612018).
- 559 [19] E. M. De La Cruz and M. L. Gardel, “Actin mechanics and fragmentation”, *Journal of*
560 *Biological Chemistry* 290 (2015), pp. 17137–17144, DOI: [10.1074/jbc.R115.636472](https://doi.org/10.1074/jbc.R115.636472).
- 561 [20] A. Zumdieck, K. Kruse, H. Bringmann, A. A. Hyman, and F. Jülicher, “Stress
562 generation and filament turnover during actin ring constriction”, *PLoS One* 2, e696
563 (2007), DOI: [10.1371/journal.pone.0000696](https://doi.org/10.1371/journal.pone.0000696).
- 564 [21] K. Kruse, J. F. Joanny, F. Jülicher, J. Prost, and K. Sekimoto, “Asters, vortices,
565 and rotating spirals in active gels of polar filaments”, *Physical Review Letters* 92,
566 078101 (2004), DOI: [10.1103/PhysRevLett.92.078101](https://doi.org/10.1103/PhysRevLett.92.078101).
- 567 [22] D. B. Oelz and A. Mogilner, “Actomyosin contraction, aggregation and traveling
568 waves in a treadmilling actin array”, *Physica D* 318–319 (2016), pp. 70–83, DOI:
569 [10.1016/j.physd.2015.10.005](https://doi.org/10.1016/j.physd.2015.10.005).
- 570 [23] F. J. Nédélec and D. Foethke, “Collective Langevin dynamics of flexible cytoskeletal
571 fibers”, *New Journal of Physics* 9, 427 (2007), DOI: [10.1088/1367-2630/9/11/427](https://doi.org/10.1088/1367-2630/9/11/427).

- 572 [24] S. L. Freedman, S. Banerjee, G. M. Hocky, and A. R. Dinner, “A versatile frame-
573 work for simulating the dynamic mechanical structure of cytoskeletal networks”,
574 *Biophysical Journal* 113 (2017), pp. 448–460, DOI: [10.1016/j.bpj.2017.06.003](https://doi.org/10.1016/j.bpj.2017.06.003).
- 575 [25] K. Popov, J. E. Komianos, and G. A. Papoian, “MEDYAN: Mechanochemical
576 simulations of contraction and polarity alignment in actomyosin networks”, *PLoS*
577 *Computational Biology* 12, e1004877 (2016), DOI: [10.1371/journal.pcbi.1004877](https://doi.org/10.1371/journal.pcbi.1004877).
- 578 [26] I. Mendes Pinto, B. Y. Rubinstein, A. Kucharavy, J. R. Unruh, and R. Li, “Actin
579 depolymerization drives actomyosin ring contraction during budding yeast cytokine-
580 sis”, *Developmental Cell* 22 (2012), pp. 1247–1260, DOI: [10.1016/j.devcel.2012.
581 04.015](https://doi.org/10.1016/j.devcel.2012.04.015).
- 582 [27] M. R. Stachowiak, C. Laplante, H. F. Chin, B. Guirao, E. Karatekin, T. D. Pollard,
583 and B. O’Shaughnessy, “Mechanism of cytokinetic contractile ring constriction in
584 fission yeast”, *Developmental Cell* 29 (2014), pp. 547–561, DOI: [10.1016/j.devcel.
585 2014.04.021](https://doi.org/10.1016/j.devcel.2014.04.021).
- 586 [28] T. Kim, “Determinants of contractile forces generated in disorganized actomyosin
587 bundles”, *Biomechanics and Modeling in Mechanobiology* 14 (2015), pp. 345–355,
588 DOI: [10.1007/s10237-014-0608-2](https://doi.org/10.1007/s10237-014-0608-2).
- 589 [29] P. Chugh, A. G. Clark, M. B. Smith, D. A. D. Cassani, K. Dierkes, A. Ragab,
590 P. P. Roux, G. Charras, G. Salbreux, and E. K. Paluch, “Actin cortex architecture
591 regulates cell surface tension”, *Nature Cell Biology* 19 (2017), pp. 689–697, DOI:
592 [10.1038/ncb3525](https://doi.org/10.1038/ncb3525).
- 593 [30] T. D. Pollard and B. O’Shaughnessy, “Molecular mechanism of cytokinesis”, *Annual*
594 *Review of Biochemistry* 88 (2019), pp. 661–689, DOI: [10.1146/annurev-biochem-
595 062917012530](https://doi.org/10.1146/annurev-biochem-062917012530).
- 596 [31] H. Ennomani, G. Letort, C. Guérin, J. Martiel, W. Cao, F. J. Nédélec, E. M. De
597 La Cruz, M. Théry, and L. Blanchoin, “Architecture and connectivity govern actin
598 network contractility”, *Current Biology* 26 (2016), pp. 616–626, DOI: [10.1016/j.
599 cub.2015.12.069](https://doi.org/10.1016/j.cub.2015.12.069).
- 600 [32] D. A. Head, A. J. Levine, and F. C. MacKintosh, “Distinct regimes of elastic
601 response and deformation modes of cross-linked cytoskeletal and semiflexible polymer
602 networks”, *Physical Review E* 68, 061907 (2003), DOI: [10.1103/PhysRevE.68.
603 061907](https://doi.org/10.1103/PhysRevE.68.061907).
- 604 [33] M. Murrell, P. W. Oakes, M. Lenz, and M. L. Gardel, “Forcing cells into shape: the
605 mechanics of actomyosin contractility”, *Nature Reviews Molecular Cell Biology* 16
606 (2015), pp. 486–498, DOI: [10.1038/nrm4012](https://doi.org/10.1038/nrm4012).

- 607 [34] T. C. Bidone, W. Jung, D. Maruri, C. Borau, R. D. Kamm, and T. Kim, “Morpho-
608 logical transformation and force generation of active cytoskeletal networks”, *PLoS*
609 *Computational Biology* 13, e1005277 (2017), DOI: [10.1371/journal.pcbi.1005277](https://doi.org/10.1371/journal.pcbi.1005277).
- 610 [35] M. Lenz, T. Thoresen, M. L. Gardel, and A. R. Dinner, “Contractile units in
611 disordered actomyosin bundles arise from F-actin buckling”, *Physical Review Letters*
612 108, 238107 (2012), DOI: [10.1103/PhysRevLett.108.238107](https://doi.org/10.1103/PhysRevLett.108.238107).
- 613 [36] K. Tawada and K. Sekimoto, “Protein friction exerted by motor enzymes through a
614 weak-binding interaction”, *Journal of Theoretical Biology* 150 (1991), pp. 193–200,
615 DOI: [10.1016/S0022-5193\(05\)80331-5](https://doi.org/10.1016/S0022-5193(05)80331-5).
- 616 [37] V. Milišić and D. B. Oelz, “On the asymptotic regime of a model for friction mediated
617 by transient elastic linkages”, *Journal de Mathématiques Pures et Appliquées* 96
618 (2011), pp. 484–501, DOI: [10.1016/j.matpur.2011.03.005](https://doi.org/10.1016/j.matpur.2011.03.005).
- 619 [38] W. M. McFadden, P. M. McCall, M. L. Gardel, and E. M. Munro, “Filament
620 turnover tunes both force generation and dissipation to control long-range flows in a
621 model actomyosin cortex”, *PLoS Computational Biology* 13, e1005811 (2017), DOI:
622 [10.1371/journal.pcbi.1005811](https://doi.org/10.1371/journal.pcbi.1005811).
- 623 [39] N. L. Dasanayake, P. J. Michalski, and A. E. Carlsson, “General mechanism of
624 actomyosin contractility”, *Physical Review Letters* 107, 118101 (2011), DOI: [10.](https://doi.org/10.1103/PhysRevLett.107.118101)
625 [1103/PhysRevLett.107.118101](https://doi.org/1103/PhysRevLett.107.118101).
- 626 [40] G. I. Bell, “Models for the specific adhesion of cells to cells”, *Science* 200 (1978),
627 pp. 618–627, DOI: [10.1126/science.347575](https://doi.org/10.1126/science.347575).
- 628 [41] G. H. Koenderink and E. K. Paluch, “Architecture shapes contractility in actomyosin
629 networks”, *Current Opinion in Cell Biology* 50 (2018), pp. 79–85, DOI: [10.1016/j.](https://doi.org/10.1016/j.ceb.2018.01.015)
630 [ceb.2018.01.015](https://doi.org/ceb.2018.01.015).
- 631 [42] A. Saha, M. Nishikawa, M. Behrndt, C. Heisenberg, F. Jülicher, and S. W. Grill,
632 “Determining physical properties of the cell cortex”, *Biophysical Journal* 110 (2016),
633 pp. 1421–1429, DOI: [10.1016/j.bpj.2016.02.013](https://doi.org/10.1016/j.bpj.2016.02.013).
- 634 [43] G. Salbreux, G. Charras, and E. Paluch, “Actin cortex mechanics and cellular
635 morphogenesis”, *Trends in Cell Biology* 22 (2012), pp. 536–545, DOI: [10.1016/j.](https://doi.org/10.1016/j.tcb.2012.07.001)
636 [tcb.2012.07.001](https://doi.org/tcb.2012.07.001).
- 637 [44] T. Kim, M. L. Gardel, and E. Munro, “Determinants of fluidlike behaviour and
638 effective viscosity in cross-linked actin networks”, *Biophysical Journal* 106 (2014),
639 pp. 526–534, DOI: [10.1016/j.bpj.2013.12.031](https://doi.org/10.1016/j.bpj.2013.12.031).

- 640 [45] M. Mak, M. H. Zaman, R. D. Kamm, and T. Kim, “Interplay of active processes modulates tension and drives phase transition in self-renewing, motor-driven cytoskeletal networks”, *Nature Communications* 7, 10323 (2016), DOI: [10.1038/ncomms10323](https://doi.org/10.1038/ncomms10323).
- 641
- 642
- 643 [46] V. Bormuth, V. Varga, J. Howard, and E. Schäffer, “Protein friction limits diffusive and directed movements of kinesin motors in microtubules”, *Science* 325 (2009), pp. 870–873, DOI: [10.1126/science.1174923](https://doi.org/10.1126/science.1174923).
- 644
- 645
- 646 [47] N. Yoshinaga and P. Marcq, “Contraction of cross-linked actomyosin bundles”, *Physical Biology* 9 (2012), DOI: [10.1088/1478-3975/9/4/046004](https://doi.org/10.1088/1478-3975/9/4/046004).
- 647
- 648 [48] A. Ward, F. Hilitski, W. Schwenger, D. Welch, A. W. C. Lau, V. Vitelli, L. Mahadevan, and Z. Dogic, “Solid friction between soft filaments”, *Nature Materials* 14 (2015), pp. 583–588, DOI: [10.1038/nmat4222](https://doi.org/10.1038/nmat4222).
- 649
- 650
- 651 [49] S. Lin, X. Han, G. C. P. Tsui, D. Hui, and L. Gu, “Active stiffening of F-actin network dominated by structural transition of actin filaments into bundles”, *Composites Part B: Engineering* 116 (2017), pp. 377–381, DOI: [10.1016/j.compositesb.2016.10.079](https://doi.org/10.1016/j.compositesb.2016.10.079).
- 652
- 653
- 654
- 655 [50] P. K. Mogensen and A. N. Risbeth, “Optim: A mathematical optimization package for Julia”, *Journal of Open Source Software* 3, 615 (2018), DOI: [10.21105/joss.00615](https://doi.org/10.21105/joss.00615).
- 656
- 657 [51] J. H. Poynting, “On pressure perpendicular to the shear planes in finite pure shears, and on the lengthening of loaded wires when twisted”, *Proceedings of the Royal Society of London, Series A, Containing Papers of a Mathematical and Physical Character* 82 (1909), pp. 546–559.
- 658
- 659
- 660
- 661 [52] M. Vahabi, B. E. Vos, H. C. G. de Cagny, D. Bonn, G. H. Koenderink, and F. C. MacKintosh, “Normal stresses in semiflexible polymer hydrogels”, *Physical Review E* 97, 032418 (2018), DOI: [10.1103/PhysRevE.97.032418](https://doi.org/10.1103/PhysRevE.97.032418).
- 662
- 663
- 664 [53] F. Gittes, B. Mickey, J. Nettleton, and J. Howard, “Flexural rigidity of microtubules and actin filaments measured from thermal fluctuations in shape”, *Journal of Cell Biology* 120 (1993), pp. 923–934, DOI: [10.1083/jcb.120.4.923](https://doi.org/10.1083/jcb.120.4.923).
- 665
- 666
- 667 [54] H. C. Berg, *Random Walks in Biology*, Princeton University Press, 1993.
- 668 [55] D. B. Oelz, U. del Castillo, V. I. Gelfand, and A. Mogilner, “Microtubule dynamics, kinesin-1 sliding, and dynein action drive growth of cell processes”, *Biophysical Journal* 115 (2018), pp. 1614–1624, DOI: [10.1016/j.bpj.2018.08.046](https://doi.org/10.1016/j.bpj.2018.08.046).
- 669
- 670
- 671 [56] T. Thoresen, M. Lenz, and M. L. Gardel, “Reconstitution of contractile actomyosin bundles”, *Biophysical Journal* 100 (2011), pp. 2698–2705, DOI: [10.1016/j.bpj.2011.04.031](https://doi.org/10.1016/j.bpj.2011.04.031).
- 672
- 673

- 674 [57] E. M. Reichl, Y. Ren, M. K. Morphew, M. Delannoy, J. C. Effler, K. D. Girard,
675 S. Divi, P. A. Iglesias, S. C. Kuo, and D. N. Robinson, “Interactions between myosin
676 and actin crosslinkers control cytokinesis contractility dynamics and mechanics”,
677 *Current Biology* 18 (2008), pp. 471–480, DOI: [10.1016/j.cub.2008.02.056](https://doi.org/10.1016/j.cub.2008.02.056).
- 678 [58] S. Stam, J. Alberts, M. L. Gardel, and E. Munro, “Isoforms confer characteristic
679 force generation and mechanosensation by myosin II filaments”, *Biophysical Journal*
680 108 (2015), pp. 1997–2006, DOI: [10.1016/j.bpj.2015.03.030](https://doi.org/10.1016/j.bpj.2015.03.030).
- 681 [59] T. Erdmann and U. S. Schwarz, “Stochastic force generation by small ensembles
682 of myosin II motors”, *Physical Review Letters* 108, 188101 (2012), DOI: [10.1103/
683 PhysRevLett.108.188101](https://doi.org/10.1103/PhysRevLett.108.188101).
- 684 [60] J. Wu and T. D. Pollard, “Counting cytokinesis proteins globally and locally in
685 fission yeast”, *Science* 310 (2005), pp. 310–314, DOI: [10.1126/science.1113230](https://doi.org/10.1126/science.1113230).
- 686 [61] F. Wang, M. Kovács, A. Hu, J. Limouze, E. V. Harvey, and J. R. Sellers, “Kinetic
687 mechanism of non-muscle myosin IIB”, *Journal of Biological Chemistry* 278 (2003),
688 pp. 27439–27448, DOI: [10.1074/jbc.M302510200](https://doi.org/10.1074/jbc.M302510200).
- 689 [62] A. Kishino and T. Yanagida, “Force measurements by micromanipulation of a single
690 actin filament by glass needles”, *Nature* 334 (1988), pp. 74–76, DOI: [10.1038/
691 334074a0](https://doi.org/10.1038/334074a0).
- 692 [63] D. B. Oelz, “A viscous two-phase model for contractile actomyosin bundles”, *Journal*
693 *of Mathematical Biology* 68 (2014), pp. 1653–1676, DOI: [10.1007/s00285-013-
694 0682-6](https://doi.org/10.1007/s00285-013-0682-6).
- 695 [64] J. M. Ferrer, H. Lee, J. Chen, B. Pelz, F. Nakamura, R. D. Kamm, and M. J. Lang,
696 “Measuring molecular rupture forces between single actin filaments and actin-binding
697 proteins”, *Proceedings of the National Academy of Science of the United States of*
698 *America* 105 (2008), pp. 9221–9226, DOI: [10.1073/pnas.0706124105](https://doi.org/10.1073/pnas.0706124105).
- 699 [65] D. H. Wachsstock, W. H. Schwarz, and T. D. Pollard, “Affinity of α -actinin for
700 actin determines the structure and mechanical properties of actin filament gels.”,
701 *Biophysical Journal* 65 (1993), pp. 205–214, DOI: [10.1016/S0006-3495\(93\)81059-2](https://doi.org/10.1016/S0006-3495(93)81059-2).
- 702 [66] W. H. Goldmann and G. Isenberg, “Analysis of filamin and α -actinin binding to
703 actin by the stopped flow method”, *Federation of European Biochemical Societies*
704 *Letters* 336 (1993), pp. 408–410, DOI: [10.1016/0014-5793\(93\)80847-N](https://doi.org/10.1016/0014-5793(93)80847-N).
- 705 [67] C. P. Descovich, D. B. Cortes, S. Ryan, J. Nash, L. Zhang, P. S. Maddox, F. J. Nédélec,
706 and A. S. Maddox, “Cross-linkers both drive and brake cytoskeletal remodeling and
707 furrowing in cytokinesis”, *Molecular Biology of the Cell* 29 (2018), pp. 622–631, DOI:
708 [10.1091/mbc.E17-06-0392](https://doi.org/10.1091/mbc.E17-06-0392).

- 709 [68] S. L. Freedman, G. M. Hocky, S. Banerjee, and A. R. Dinner, “Nonequilibrium
710 phase diagrams for actomyosin networks”, *Soft Matter* 14 (2018), pp. 7740–7747,
711 DOI: [10.1039/c8sm00741a](https://doi.org/10.1039/c8sm00741a).
- 712 [69] F. J. Nédélec, T. Surrey, A. C. Maggs, and S. Leibler, “Self-organisation of micro-
713 tubules and motors”, *Nature* 389 (1997), pp. 305–308, DOI: [10.1038/38532](https://doi.org/10.1038/38532).
- 714 [70] M. R. Stachowiak, P. M. McCall, T. Thoresen, H. E. Balcioglu, L. Kasiewicz, M. L.
715 Gardel, and B. O’Shaughnessy, “Self-organization of myosin II in reconstituted
716 actomyosin bundles”, *Biophysical Journal* 103 (2012), pp. 1265–1274, DOI: [10.1016/
717 j.bpj.2012.08.028](https://doi.org/10.1016/j.bpj.2012.08.028).
- 718 [71] E. W. Weisstein, *Square Line Picking*, MathWorld — a Wolfram Web Resource,
719 URL: <https://mathworld.wolfram.com/SquareLinePicking.html>.
- 720 [72] A. C. Martin, M. Kaschube, and E. F. Wieschaus, “Pulsed contractions of an actin–
721 myosin network drive apical constriction”, *Nature* 457 (2009), pp. 495–499, DOI:
722 [10.1038/nature07522](https://doi.org/10.1038/nature07522).
- 723 [73] L. He, X. Wang, H. L. Tang, and D. J. Montell, “Tissue elongation requires oscillating
724 contractions of a basal actomyosin network”, *Nature Cell Biology* 12 (2010), pp. 1133–
725 1142, DOI: [10.1038/ncb2124](https://doi.org/10.1038/ncb2124).
- 726 [74] Q. Yu, J. Li, M. P. Murrell, and T. Kim, “Balance between force generation and
727 relaxation leads to pulsed contraction of actomyosin networks”, *Biophysical Journal*
728 115 (2018), pp. 2003–2013, DOI: [10.1016/j.bpj.2018.10.008](https://doi.org/10.1016/j.bpj.2018.10.008).
- 729 [75] S. Pellegrin and H. Mellor, “Actin stress fibres”, *Journal of Cell Science* 120 (2007),
730 pp. 3491–3499, DOI: [10.1242/jcs.018473](https://doi.org/10.1242/jcs.018473).
- 731 [76] J. Alvarado, M. Sheinman, A. Sharma, F. C. MacKintosh, and G. H. Koenderink,
732 “Molecular motors robustly drive active gels to a critically connected state”, *Nature*
733 *Physics* 9 (2013), pp. 591–597, DOI: [10.1038/nphys2715](https://doi.org/10.1038/nphys2715).
- 734 [77] C. Scheibner, A. Souslov, D. Banerjee, P. Surówka, W. M. T. Irvine, and V. Vitelli,
735 “Odd elasticity”, *Nature Physics* 16 (2020), pp. 475–480, DOI: [10.1038/s41567-020-
736 0795-y](https://doi.org/10.1038/s41567-020-0795-y).

Supporting Material: Protein Friction and Filament Bending Facilitate Contraction of Disordered Actomyosin Networks

Alexander K. Y. Tam^{*1}, Alex Mogilner², and Dietmar B. Oelz¹

¹School of Mathematics and Physics, The University of Queensland, St Lucia, Queensland 4072, Australia

²Courant Institute of Mathematical Sciences, New York University, New York, NY 10012, USA

June 18, 2021

A Mathematical Model Derivation

We develop and implement an agent-based mathematical model for two-dimensional actomyosin networks. We represent actin filaments as finite-length curves in \mathbb{R}^2 , and to track their position introduce the variables $z_i(s(t), t) \in \mathbb{R}^2$ for $i = 1, \dots, N_a$, where N_a is the number of semi-flexible actin filaments. These represent the physical position of the actin filament, parameterised by the arc length $s(t) \in [0, L_i]$, where L_i is the length of the i -th actin filament. We consider a simplified representation of myosin motors as dumbbells that behave like stiff linear springs. The two ends of the dumbbell represent motor ‘heads’ that bind to actin filaments and exert forces. To track motor head positions, we define the variables $m_{ik}(t) \in [0, L_i]$, for $k = 1, \dots, N_m$, where N_m is the number of myosin motors. These are the positions (measured from the minus end) of the k -th myosin motor along the actin filament with index i , to which it is bound. The derivation of our model in a time-discrete context then involves constructing an energy functional that depends on the degrees of freedom z_i and m_{ik} . At each time step, the solution is given by the minimiser of this functional, and advancing in time enables us to simulate network evolution. We solve the model on a two-dimensional domain with periodic boundary conditions, such that the network evolves on the surface of a torus.

A.1 Energy Functional

We write the mathematical model in a time-discrete context in terms of an energy functional that depends on the degrees of freedom $z_i(s(t), t)$, and $m_{ik}(t)$. This functional **contains**

^{*}Corresponding author: alex.tam@uq.edu.au

contributions from each mechanical feature in the model. It combines the potential energy contributions for filament bending and filament and motor spring forces, with pseudo-energy terms whose variations correspond to finite-difference approximations of the thermal, drag, protein friction, and motor forces acting on filaments. At each time step of the simulation, the network evolves to minimise this energy functional. In abstract terms, the energy functional for the network is

$$E_{\text{net}} := E_{a,\text{drag}} + E_{a,\text{bend}} + E_{a,\text{spring}} + E_{a,\text{pf}} + E_{m,\text{spring}} + E_{m,a}, \quad (\text{A.1})$$

where the subscripts a and m refer to actin and myosin respectively. Below, we outline the meaning and mathematical description of each term in (A.1).

We assume that viscous drag with a background medium resists motion of the actin filaments. We then obtain the pseudo-energy contribution for actin drag,

$$E_{a,\text{drag}} = \sum_{i=1}^{N_a} \int_0^{L_i} \frac{\lambda_a}{2\Delta t} |z_i - \mathbf{F} z_i^n|^2 ds_i. \quad (\text{A.2})$$

In (A.2), λ_a is the coefficient of viscous drag for actin–background interactions, and is similar to the damping term λ in the Langevin equation. The vector z_i^n represents filament positions at the previous time step, where Δt is the time step size. To account for stretching and rotation of the domain, we multiply z_i^n by the deformation gradient tensor

$$\mathbf{F} = \begin{bmatrix} L_{xx}/L_{xx}^n & L_{yx}/L_{yy}^n \\ L_{xy}/L_{xx}^n & L_{yy}/L_{yy}^n \end{bmatrix}, \quad (\text{A.3})$$

which ensures both z_i and z_i^n are represented in the current spatial co-ordinates. In network-scale simulations, this drag term represents hydrodynamic drag with the background cytoplasm. An alternative interpretation of viscous drag is to assume that the simulated network is a subset of a dense, homogeneous, cross-linked network of filaments.

Since filaments are semi-flexible, we also include the contribution of elastic potential energy due to bending. This is given by

$$E_{a,\text{bend}} = \sum_{i=1}^{N_a} \int_0^{L_i} \frac{\kappa_a}{2} |z_i''|^2 ds_i, \quad (\text{A.4})$$

where κ_a is the flexural rigidity, assumed constant for all actin filaments. The third term in (A.1), $E_{a,\text{spring}}$, is the energy associated with local longitudinal extension of actin filaments.

According to Hooke's law, after summing the contributions of all filaments, it is given by

$$E_{a,\text{spring}} = \sum_{i=1}^{N_a} \int_0^{L_i} \frac{\tilde{k}_a}{2} (|z'_i| - 1)^2 ds_i, \quad (\text{A.5})$$

where $\tilde{k}_a = k_a \Delta s$, where Δs is the segment length used in the numerical discretisation. We assume the longitudinal stiffness, k_a , to be the same for all filaments. Note that in the context of our model we regard (A.5) as a penalising potential with large coefficient k_a in order to model actin filament inextensibility and to regard s_i as an arc-length parametrisation.

Protein friction between actin filaments also contributes to the energy functional. In our model, we represent this as a viscous drag contribution that acts point-wise at intersections between actin filaments. This viscous force can arise due to contact friction between overlapping filaments [1], or as the macroscopic effect of abundant cross-linkers that undergo turnover [2]. The pseudo-energy contribution due to protein friction is

$$E_{a,\text{pf}} = \sum_{i=1}^{N_a} \sum_{\substack{j=1 \\ j>i}}^{N_a} A_{ij} \frac{\lambda_{\text{pf}}}{2\Delta t} d(z_i(\alpha_{ij}, t), z_j(\alpha_{ji}, t))^2, \quad (\text{A.6})$$

where λ_{pf} is the protein friction drag coefficient. In (A.6), A_{ij} is a binary variable such that $A_{ij} = 1$ if filaments i and j intersect and no motor is bound to both filaments, and $A_{ij} = 0$ otherwise. We also define $d(z_1, z_2)$ to be the shortest physical distance between two points $z_1, z_2 \in \mathbb{R}^2$ or their periodic translations, enabling us to account for periodic boundary conditions. Finally, $\alpha_{ij} \in [0, L_i]$ is the position along filament i at which the intersection with filament j occurs, and ensures that protein friction drag is applied point-wise at these intersections.

The final two terms in (A.1) model the effects of myosin motors. In the same way as we account for F-actin inextensibility, we use the penalising potential

$$E_{m,\text{spring}} = \sum_{i=1}^{N_a} \sum_{\substack{j=1 \\ j>i}}^{N_a} \sum_{k=1}^{N_m} \theta_{ijk} \frac{k_m}{2} d(z_i(m_{ik}, t), z_j(m_{jk}, t))^2, \quad (\text{A.7})$$

to model myosin inextensibility. Here k_m is the myosin motor spring constant which we take as very large, and θ_{ijk} is a binary variable such that $\theta_{ijk} = 1$ if myosin motor k is attached to filaments i and j , and $\theta_{ijk} = 0$ otherwise. The final term in (A.1) describes interactions between filaments and motors. We assume that myosin obeys a linear force-velocity

relation, such that positions evolve according to

$$\frac{dm_{ik}}{dt} = V_m \left(1 - \frac{F_k}{F_s} \right), \quad (\text{A.8})$$

where V_m is the load-free myosin motor velocity, F_s is the motor stall force, and $F_k = k_m [z_i(m_{ik}, t) - z_j(m_{jk}, t)] \cdot z'_i$ is the projection of the spring force through the k -th myosin motor onto the direction of the i -th filament. To reproduce (A.8) as the variation of a pseudo-energy, we introduce a linear term for the load-free velocity, and a quadratic term with the same scaling as the drag terms above for the linear velocity reduction due to motor loading. The pseudo-energy then reads

$$E_{m,a} = - \sum_{i=1}^{N_a} \sum_{k=1}^{N_m} \theta_{ik} \left[F_s (m_{ik} - m_{ik}^n) - \frac{F_s}{V_m} \frac{(m_{ik} - m_{ik}^n)^2}{2\Delta t} \right], \quad (\text{A.9})$$

where θ_{ik} is a binary variable such that $\theta_{ik} = 1$ if motor k is attached to filament i , and $\theta_{ik} = 0$ otherwise. This completes the description of all terms in the network energy functional.

A.2 Stochastic Filament and Motor Turnover

We simulate random actin filament turnover and myosin motor unbinding. Given an off-rate k_{off} , the probability of turnover or detachment in a given time step according to an exponential distribution is

$$p_{\text{off}} = 1 - e^{-k_{\text{off}}\Delta t}, \quad (\text{A.10})$$

where Δt is the time step size. We assume that the turnover rate for actin filaments, $k_{\text{off},a}$, is constant and the same for each filament. At each time step, we use a pseudo-random number generator to simulate whether each filament will turn over. To maintain constant filament density, we immediately replace filaments that turn over with new ones at random positions and orientations. If a filament turns over, we also assume that any myosin motor attached to the filament automatically unbinds.

In contrast, we assume that the unbinding rate for myosin motors depends on the force it experiences. According to Bell's law, the force-dependent unbinding rate is given by

$$k_m = k_{\text{off},m} e^{F/F_{\text{ref}}}, \quad (\text{A.11})$$

where $k_{\text{off},m}$ is the reference off-rate for unloaded motors, and F_{ref} is a reference force. The force to which the k -th motor is subject is the variation of the penalising potential (A.7) and given by a Hooke's law, where motors are assumed to be linear springs with equilibrium length zero. This yields $F_k = k_m d(z_i(m_{ik}, t) - z_j(m_{jk}, t))$, where i and j are

the indices of the two filaments to which the motor attaches, such that the distance term measures the motor length. Like the actin filaments, we maintain constant myosin motor density throughout the simulation by assuming that an unbound motor is immediately replaced with a new one at a random filament intersection.

A.3 Parameters

We performed network simulations in the main text with a set of default parameters. These parameters are listed in Table A.1. Additional information on the derivation of

Table A.1: Default parameters for actomyosin network simulations.

Parameter	Symbol	Value	Units	Source
Longitudinal stiffness (actin)	k_a	1000	$\text{pN } \mu\text{m}^{-1}$	[3]
Longitudinal stiffness (myosin)	k_m	1000	$\text{pN } \mu\text{m}^{-1}$	[3]
Actin filament flexural rigidity	κ_a	0.073	$\text{pN } \mu\text{m}^2$	[4]
Equilibrium actin filament length	L_a	1	μm	[5–7]
Actin–cytoplasm drag coefficient	λ_a	0.05	$\text{pN } \mu\text{m}^{-2} \text{ s}$	[8–10]
Protein friction drag coefficient	λ_{pf}	30	$\text{pN } \mu\text{m}^{-1} \text{ s}$	[1]
Myosin stall force	F_s	5	pN	[11–13]
Myosin free-moving velocity	V_m	0.5	$\mu\text{m s}^{-1}$	[11, 13, 14]
Actin filament turnover rate	$k_{\text{off},a}$	0.04	s^{-1}	[15, 16]
Myosin reference off-rate	$k_{\text{off},m}$	0.35	s^{-1}	[17, 18]
Myosin reference unbinding force	F_{ref}	12.6	pN	[19]
Number of actin filaments	N_a	50	[–]	Assumption
Number of myosin motors	N_m	10	[–]	Assumption
Domain width	L_{xx}, L_{yy}	2.5	μm	Assumption
Simulation duration	T	60	s	Assumption

some parameters is provided below.

Longitudinal Stiffnesses, k_a, k_m : We assume that actin filament segments and myosin motors are stiff entities, and following Stachowiak et al. [3] use $k_a = k_m = 1000 \text{ pN } \mu\text{m}^{-1}$. Although our chosen value for k_a is smaller than the value $k_a = 34.5 \text{ pN nm}^{-1}$ observed in experiments by Liu and Pollack [20], by inspection our choices are sufficiently large to ensure filament segments and myosin motors experience negligible extension. A lower value of k_a also accounts for the low-tension regime, where actin filaments are more compliant than when under high tension [20].

Actin Filament Length: Actin filament length depends on cell type and function, and can vary across experiments. Since our modelling follows Dasanayake, Michalski, and Carlsson [6] and Hiraiwa and Salbreux [7], we adapt estimates from these authors. Dasanayake,

Michalski, and Carlsson [6] use $L_a = 2 \mu\text{m}$, whereas Hiraiwa and Salbreux [7] use $L_a = 0.1\text{--}1 \mu\text{m}$. Experimental measurements of fission yeast by Kamasaki, Osumi, and Mabuchi [5] give $L_a = 0.6 \mu\text{m}$, and Stachowiak et al. [3] use $L_a = 1.3 \mu\text{m}$. Based on this data, a reasonable estimate for our model is $L_a = 1 \mu\text{m}$.

Actin–background drag coefficient, λ_a : Since the actin–background drag coefficient is difficult to estimate, we assume $\lambda_a = 0.05 \text{ pN } \mu\text{m}^{-2} \text{ s}$ in network simulations. This value is small enough that actin–background drag has **only a minor** effect on the network. For an experimental justification of this parameter, we **follow Oelz et al. [9], who adapt a formula from Berg [8] to obtain**

$$\lambda_a = \frac{3\pi\eta}{\log(2a/b)}, \quad (\text{A.12})$$

where η is the viscosity of the medium (in this case the cytoplasm), a is the semi-major axis length (*i.e.* half the filament length), and b is the semi-minor axis length (*i.e.* the actin filament radius). We assume filaments have the constant length $L_a = 1 \mu\text{m}$, and thus $a = 0.5 \mu\text{m}$. The actin filament has a diameter of 7 nm [21], such that the radius is $b = 0.0035 \mu\text{m}$. The drag coefficient $\lambda_a = 0.05 \text{ pN s } \mu\text{m}^{-2}$ then corresponds to $\eta = 0.03 \text{ pN s } \mu\text{m}^{-2}$, which is approximately 30 times the viscosity of water.

Protein Friction Drag Coefficient, λ_{pf} : We estimate the protein friction drag coefficient using experimental work by Ward et al. [1] on sliding friction between F-actin filaments. Given a pulling velocity of $0.2 \mu\text{m s}^{-1}$, they obtain a frictional force of approximately 6 pN , suggesting that $\lambda_{\text{pf}} = 30 \text{ pN } \mu\text{m}^{-1} \text{ s}$.

Under the alternative interpretation of protein friction as the macroscopic effect of abundant, transient cross-linkers, we can estimate λ_{pf} by modifying the formula used by Oelz [22]. We then have

$$\lambda_{\text{pf}} = k_\alpha \rho_\alpha s_\alpha L_\alpha \mu_{1,0,\alpha} \quad (\text{A.13})$$

where k_α is the spring stiffness constant of the cross-linker (α -actinin), ρ_α is the maximal cross-linker density, s_α is a saturation factor, L_α is the cross-linker length, and $\mu_{1,0} = 1/(\zeta(1 + \zeta/\beta))$ is a parameter that incorporates the on-rate, β , and off-rate, ζ , of the cross-linker, as derived in Milišić and Oelz [2]. Ferrer et al. [23] give $k_\alpha = 100 \text{ pN } \mu\text{m}^{-1}$, and Oelz [22] estimate that $\rho_\alpha = 70 \mu\text{m}^{-1}$ and $s_\alpha = 0.05$. The length of α -actinin is $L_\alpha = 36 \text{ nm}$ [24]. From Goldmann and Isenberg [25], we obtain an on-rate of $\beta = 1 \text{ s}^{-1}$, if we assume that the concentration of α -actinin is $1 \mu\text{M}$. Goldmann and Isenberg [25] also claim that $\zeta = 0.44 \text{ s}^{-1}$, allowing us to compute $\mu_{1,0,\alpha} = 1.5783 \text{ s}$. Thus, $\lambda_{\text{pf}} = 19.89 \text{ pN } \mu\text{m}^{-1} \text{ s}$. This is similar in magnitude to the estimate from Ward et al. [1].

Myosin Reference Off-Rate, $k_{\text{off},m}$: Stam et al. [17], citing Wang et al. [18], state that the reference off-rate $k_{\text{off}}(0)$ for non-muscle myosin is 0.35 s^{-1} (IIA) and 1.71 s^{-1} (IIB). This parameter therefore depends on the isoform of the myosin, and we adopt the value for myosin-IIA.

Actin Turnover Rate, $k_{\text{off},a}$: In the cell cortex, Saha et al. [15] estimate the timescale for actin filament turnover to be approximately 25 s for *C. elegans*. Based on this, we will use a turnover rate of $k_{\text{off},a} = 0.04 \text{ s}^{-1}$ in our simulations.

B Numerical Simulations and Performance Information

This appendix contains information about the numerical algorithm, including its performance, convergence, and the effect of thermal forces.

B.1 Effect of Thermal Forces

Random filament movement due to thermal fluctuations is commonly included in mathematical models for actomyosin networks. This involves adding the thermal force term $\mathbf{F}_{a,\text{therm}}$ to the force balance equations,

$$\begin{aligned} \mathbf{o} = & \mathbf{F}_{a,\text{therm}} + \mathbf{F}_{a,\text{drag}} - \delta E_{a,\text{bend}} - \delta E_{a,\text{spring}} + \mathbf{F}_{a,\text{pf}} \\ & - \delta E_{m,\text{spring}} + \mathbf{F}_{m,a}. \end{aligned} \quad (\text{B.1})$$

In the time-discrete formulation of (B.1) in which we represent filament k as a sequence of nodes with indices i , the thermal force term applied to each node is

$$\mathbf{F}_{a,\text{therm}}^{k,i} := \sqrt{\frac{2k_b T \lambda_a \bar{l}_{k,i}^n}{\Delta t}} \theta_{k,i}^n. \quad (\text{B.2})$$

In (B.2), $k_b = 1.38 \times 10^{-5} \text{ } \mu\text{m pN K}^{-1}$ is the Boltzmann constant, T is the temperature (assumed to be 298.15 K), $\bar{l}_{k,i}^n$ is the mean length of the two filament segments adjacent to the node i of filament k at time n (or half the length of the first or last segment for minus and plus-end nodes respectively), and $\theta_{k,i}^n$ is a random vector sampled with the standard normal distribution.

To investigate how these affect our results, we performed 25 simulations with thermal fluctuations included. Bulk stress results from these simulations are presented in the box plots in Figure B.1. These results confirm that thermal fluctuations have little effect on stress. Indeed, for rigid filaments their effect is negligible. In semi-flexible networks, thermal fluctuations can generate stochastic filament bending, which might cause increased

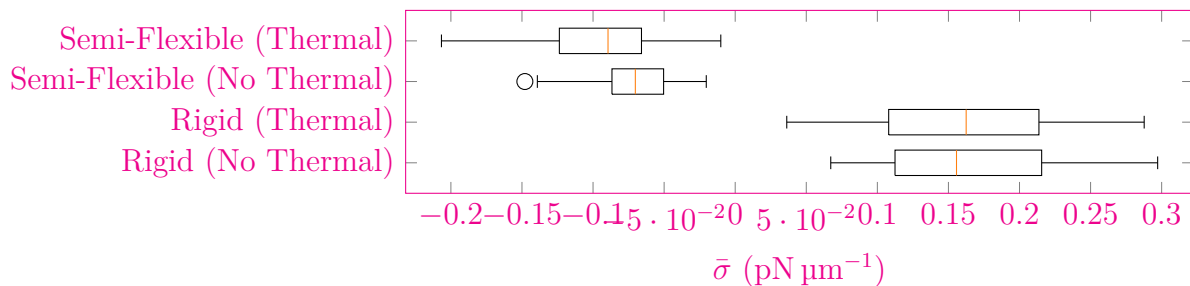


Figure B.1: Box plots comparing the bulk stress in 25 simulations of disordered networks.

contractility. However, the results presented in Figure B.1 confirm that stochastic bending effects are minor. Therefore, we omit thermal fluctuations from the main results presented in the paper, to emphasise protein friction and motor-induced bending as mechanisms of contraction.

B.2 Effect of Simulation Domain Size

Next, we performed 10 simulations on a larger ($5 \mu\text{m} \times 5 \mu\text{m}$) domain, to confirm that the domain size and periodic boundary conditions do not affect the results. To maintain the same density of filaments and motors, for each larger simulation we used 200 filaments and 40 motors. We compare bulk stress results for these large-domain simulations with the default simulations in Figure B.2. These confirm that the domain size and periodic

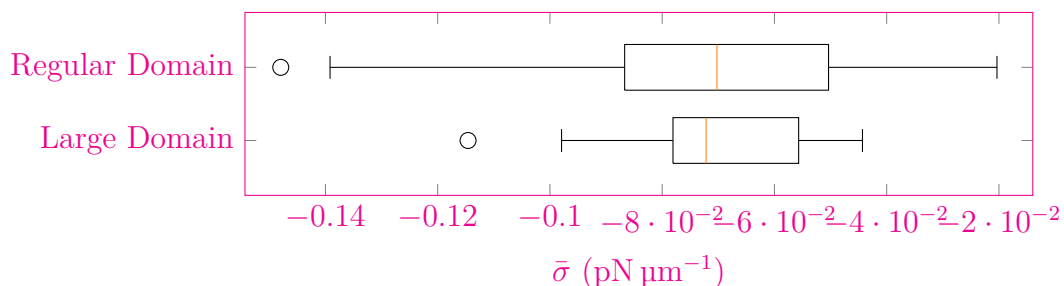


Figure B.2: Box plots comparing the bulk stress in simulations on the regular domain used throughout the manuscript, and a larger domain of size $5 \mu\text{m} \times 5 \mu\text{m}$.

boundary have no discernible effect on mean bulk stress $\bar{\sigma}$. Since the large-domain simulations aggregate forces for more filaments and motors than the regular-domain simulations, they exhibit variation in stress across the simulations.

B.3 Effect of System Size on Performance

The following plots describe how the simulation time and memory usage vary with the system size. In each simulation, we use the parameters from Table A.1, and compute

the time and memory requirements for 100 time steps with $\Delta t = 0.05$ s. The simulations were performed using a Dell Optiplex 7060 i7-8700 desktop computer, with a 3.2GHz 6-core CPU and 15.4GB RAM, running the Linux Mint 20.1 (Cinnamon) operating system. We perform the energy minimisation using the LBFGS method from `Optim.jl`, and use `AutoDiff.jl` to evaluate the gradient.

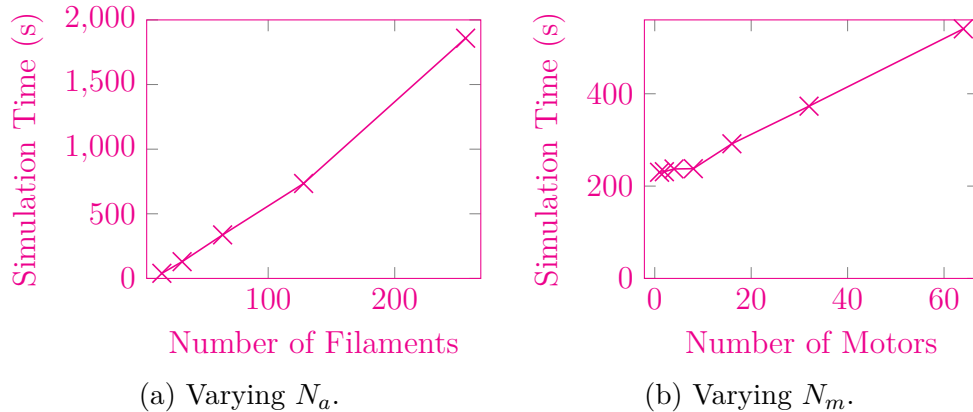


Figure B.3: Effect of system size on simulation time. Simulations in (a) varying the number of filaments were performed using $N_m = 5$ myosin motors. Simulations in (b) varying the number of myosin motors were performed using $N_a = 50$ actin filaments.

B.4 Effect of Time Step Size on Performance

We also investigated how the time step size affects performance. In Figure B.4, we vary Δt , and measure the time to simulate a random network to $T = 5$ s. All other parameters are as in Table A.1, and the same computer was used as in §B.3. An advantage of

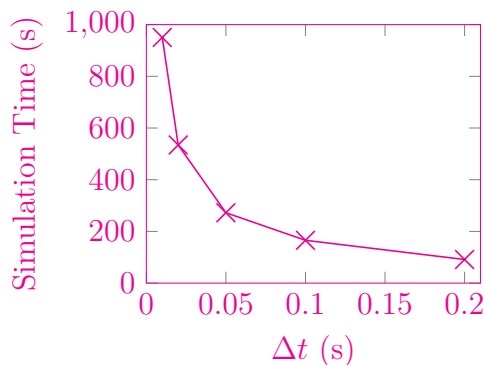


Figure B.4: Effect of time step size on simulation time.

our time-implicit numerical method is that we can take large time steps without loss of numerical stability. However, as Figure B.4 shows, the marginal performance improvement diminishes as we increase Δt . This is because the optimisation routine uses the previous

time step as its initial guess. For smaller time steps, the solution will be closer to this initial guess, enabling the optimisation routine to converge faster at each step. Our results were computed with $\Delta t = 0.05$ s, which ensured that solutions were independent of Δt .

B.5 Effect of Optimisation Routine Tolerance on Performance

The `Optim.jl` package enables users to specify the tolerance, ε , that determines when the routine considers the optimisation to have converged. Figure B.5 shows how this tolerance affects the time to simulate 101 time steps with $\Delta t = 0.05$ s, and default parameters from Table A.1. As expected, decreasing the tolerance increases the speed of simulation. Our results were computed with $\varepsilon = 1 \times 10^{-8}$, which was sufficiently small such that solutions were independent of ε .

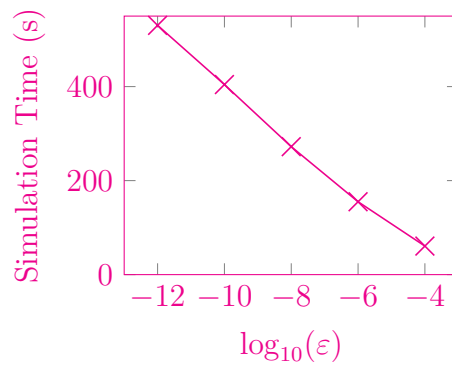


Figure B.5: Effect of optimisation routine tolerance on simulation time.

C Filament Aggregation Results

The following series of plots contains the final network configurations and distance distributions for the ten simulations performed with $T = 300$ s, and both $k_{\text{off},a} = 0 \text{ s}^{-1}$ and $k_{\text{off},a} = 0.2 \text{ s}^{-1}$.

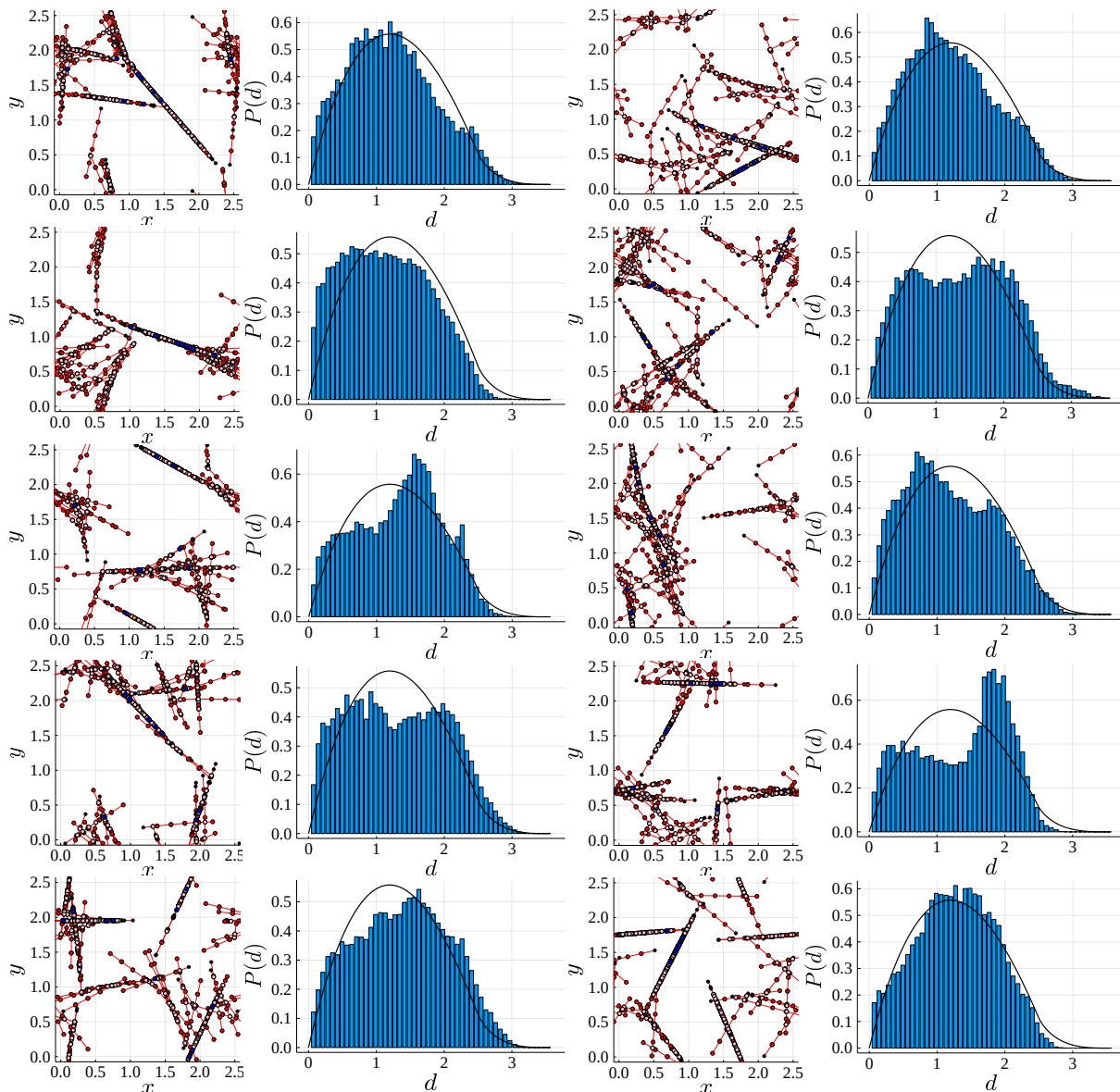


Figure C.1: Final network configurations at $t = 300$ s and histograms of the distances between pairs of nodes on different filaments. Results presented for ten simulations with $k_{\text{off},a} = 0 \text{ s}^{-1}$.

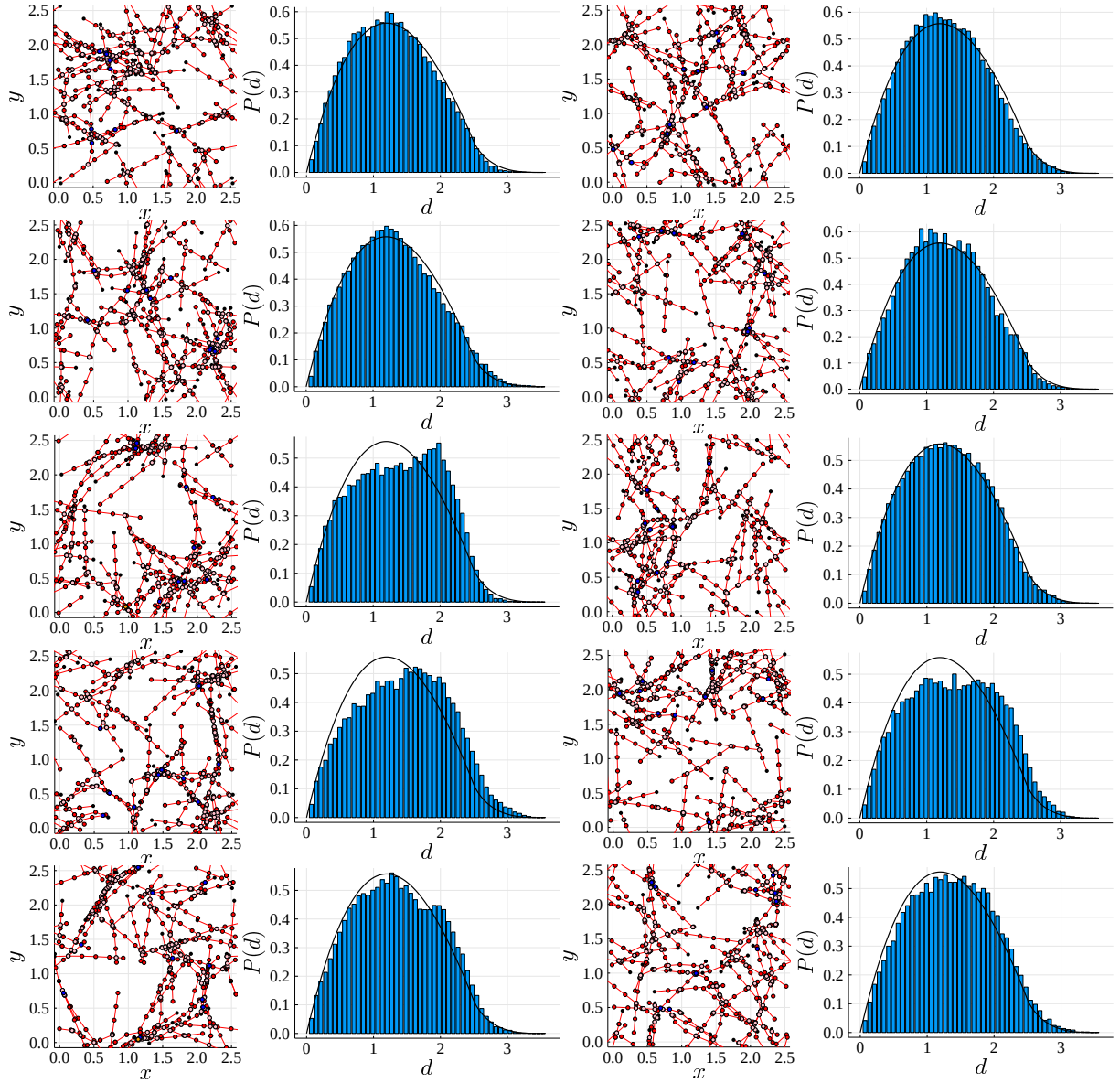


Figure C.2: Final network configurations at $t = 300$ s and histograms of the distances between pairs of nodes on different filaments. Results presented for ten simulations with $k_{\text{off},a} = 0.2 \text{ s}^{-1}$.

References

- [1] A. Ward, F. Hilitski, W. Schwenger, D. Welch, A. W. C. Lau, V. Vitelli, L. Mahadevan, and Z. Dogic, “Solid friction between soft filaments”, *Nature Materials* 14 (2015), pp. 583–588, DOI: [10.1038/nmat4222](https://doi.org/10.1038/nmat4222).
- [2] V. Milišić and D. B. Oelz, “On the asymptotic regime of a model for friction mediated by transient elastic linkages”, *Journal de Mathématiques Pures et Appliquées* 96 (2011), pp. 484–501, DOI: [10.1016/j.matpur.2011.03.005](https://doi.org/10.1016/j.matpur.2011.03.005).
- [3] M. R. Stachowiak, C. Laplante, H. F. Chin, B. Guirao, E. Karatekin, T. D. Pollard, and B. O’Shaughnessy, “Mechanism of cytokinetic contractile ring constriction in fission yeast”, *Developmental Cell* 29 (2014), pp. 547–561, DOI: [10.1016/j.devcel.2014.04.021](https://doi.org/10.1016/j.devcel.2014.04.021).
- [4] F. Gittes, B. Mickey, J. Nettleton, and J. Howard, “Flexural rigidity of microtubules and actin filaments measured from thermal fluctuations in shape”, *Journal of Cell Biology* 120 (1993), pp. 923–934, DOI: [10.1083/jcb.120.4.923](https://doi.org/10.1083/jcb.120.4.923).
- [5] T. Kamasaki, M. Osumi, and I. Mabuchi, “Three-dimensional arrangement of F-actin in the contractile ring of fission yeast”, *Journal of Cell Biology* 178 (2007), pp. 765–771, DOI: [10.1083/jcb.200612018](https://doi.org/10.1083/jcb.200612018).
- [6] N. L. Dasanayake, P. J. Michalski, and A. E. Carlsson, “General mechanism of actomyosin contractility”, *Physical Review Letters* 107, 118101 (2011), DOI: [10.1103/PhysRevLett.107.118101](https://doi.org/10.1103/PhysRevLett.107.118101).
- [7] T. Hiraiwa and G. Salbreux, “Role of turnover in active stress generation in a filament network”, *Physical Review Letters* 116, 188101 (2016), DOI: [10.1103/PhysRevLett.116.188101](https://doi.org/10.1103/PhysRevLett.116.188101).
- [8] H. C. Berg, *Random Walks in Biology*, Princeton University Press, 1993.
- [9] D. B. Oelz, U. del Castillo, V. I. Gelfand, and A. Mogilner, “Microtubule dynamics, kinesin-1 sliding, and dynein action drive growth of cell processes”, *Biophysical Journal* 115 (2018), pp. 1614–1624, DOI: [10.1016/j.bpj.2018.08.046](https://doi.org/10.1016/j.bpj.2018.08.046).
- [10] T. Kim, M. L. Gardel, and E. Munro, “Determinants of fluidlike behaviour and effective viscosity in cross-linked actin networks”, *Biophysical Journal* 106 (2014), pp. 526–534, DOI: [10.1016/j.bpj.2013.12.031](https://doi.org/10.1016/j.bpj.2013.12.031).
- [11] D. B. Oelz, B. Y. Rubinstein, and A. Mogilner, “A combination of actin treadmilling and cross-linking drives contraction of random actomyosin arrays”, *Biophysical Journal* 109 (2015), pp. 1818–1829, DOI: [10.1016/j.bpj.2015.09.013](https://doi.org/10.1016/j.bpj.2015.09.013).

- [12] T. Thoresen, M. Lenz, and M. L. Gardel, “Reconstitution of contractile actomyosin bundles”, *Biophysical Journal* 100 (2011), pp. 2698–2705, DOI: [10.1016/j.bpj.2011.04.031](https://doi.org/10.1016/j.bpj.2011.04.031).
- [13] E. M. Reichl, Y. Ren, M. K. Morphew, M. Delannoy, J. C. Effler, K. D. Girard, S. Divi, P. A. Iglesias, S. C. Kuo, and D. N. Robinson, “Interactions between myosin and actin crosslinkers control cytokinesis contractility dynamics and mechanics”, *Current Biology* 18 (2008), pp. 471–480, DOI: [10.1016/j.cub.2008.02.056](https://doi.org/10.1016/j.cub.2008.02.056).
- [14] J. Wu and T. D. Pollard, “Counting cytokinesis proteins globally and locally in fission yeast”, *Science* 310 (2005), pp. 310–314, DOI: [10.1126/science.1113230](https://doi.org/10.1126/science.1113230).
- [15] A. Saha, M. Nishikawa, M. Behrndt, C. Heisenberg, F. Jülicher, and S. W. Grill, “Determining physical properties of the cell cortex”, *Biophysical Journal* 110 (2016), pp. 1421–1429, DOI: [10.1016/j.bpj.2016.02.013](https://doi.org/10.1016/j.bpj.2016.02.013).
- [16] A. Zumdick, K. Kruse, H. Bringmann, A. A. Hyman, and F. Jülicher, “Stress generation and filament turnover during actin ring constriction”, *PLoS One* 2, e696 (2007), DOI: [10.1371/journal.pone.0000696](https://doi.org/10.1371/journal.pone.0000696).
- [17] S. Stam, J. Alberts, M. L. Gardel, and E. Munro, “Isoforms confer characteristic force generation and mechanosensation by myosin II filaments”, *Biophysical Journal* 108 (2015), pp. 1997–2006, DOI: [10.1016/j.bpj.2015.03.030](https://doi.org/10.1016/j.bpj.2015.03.030).
- [18] F. Wang, M. Kovács, A. Hu, J. Limouze, E. V. Harvey, and J. R. Sellers, “Kinetic mechanism of non-muscle myosin IIB”, *Journal of Biological Chemistry* 278 (2003), pp. 27439–27448, DOI: [10.1074/jbc.M302510200](https://doi.org/10.1074/jbc.M302510200).
- [19] T. Erdmann and U. S. Schwarz, “Stochastic force generation by small ensembles of myosin II motors”, *Physical Review Letters* 108, 188101 (2012), DOI: [10.1103/PhysRevLett.108.188101](https://doi.org/10.1103/PhysRevLett.108.188101).
- [20] X. Liu and G. H. Pollack, “Mechanics of F-actin characterized with microfabricated cantilevers”, *Biophysical Journal* 83 (2002), pp. 2705–2715, DOI: [10.1016/S0006-3495\(02\)75280-6](https://doi.org/10.1016/S0006-3495(02)75280-6).
- [21] A. Kishino and T. Yanagida, “Force measurements by micromanipulation of a single actin filament by glass needles”, *Nature* 334 (1988), pp. 74–76, DOI: [10.1038/334074a0](https://doi.org/10.1038/334074a0).
- [22] D. B. Oelz, “A viscous two-phase model for contractile actomyosin bundles”, *Journal of Mathematical Biology* 68 (2014), pp. 1653–1676, DOI: [10.1007/s00285-013-0682-6](https://doi.org/10.1007/s00285-013-0682-6).

- [23] J. M. Ferrer, H. Lee, J. Chen, B. Pelz, F. Nakamura, R. D. Kamm, and M. J. Lang, “Measuring molecular rupture forces between single actin filaments and actin-binding proteins”, *Proceedings of the National Academy of Science of the United States of America* 105 (2008), pp. 9221–9226, DOI: [10.1073/pnas.0706124105](https://doi.org/10.1073/pnas.0706124105).
- [24] D. H. Wachsstock, W. H. Schwarz, and T. D. Pollard, “Affinity of α -actinin for actin determines the structure and mechanical properties of actin filament gels.”, *Biophysical Journal* 65 (1993), pp. 205–214, DOI: [10.1016/S0006-3495\(93\)81059-2](https://doi.org/10.1016/S0006-3495(93)81059-2).
- [25] W. H. Goldmann and G. Isenberg, “Analysis of filamin and α -actinin binding to actin by the stopped flow method”, *Federation of European Biochemical Societies Letters* 336 (1993), pp. 408–410, DOI: [10.1016/0014-5793\(93\)80847-N](https://doi.org/10.1016/0014-5793(93)80847-N).